BOSTON UNIVERSITY
COLLEGE OF ENGINEERING

Dissertation

DENSITY RELAXATION AND IMPURITY INCORPORATION IN THIN SILICON DIOXIDE FILMS AND THEIR EFFECTS ON BORON DIFFUSION

by

Mitra Navi

B.S., FITCHBURG STATE COLLEGE, 1988
M.S., BOSTON UNIVERSITY, 1993

Submitted in partial fulfillment of the
requirements for the degree of
Doctor of Philosophy
1998

Approved by

First Reader

Scott T. Dunham, Ph.D.
Professor of Electrical Engineering

Second Reader

Theodore D. Moustakas, Ph.D.
Professor of Electrical Engineering

Third Reader

M. Selim Ünlü, Ph.D.
Professor of Electrical Engineering

Fourth Reader

Michael Yeung, Ph.D.
Professor of Manufacturing Engineering

Acknowledgements

I wish to thank my advisor, Professor Scott Dunham, for his guidance and support during my many years at Boston University. I truly appreciate the opportunities he has given me to explore my interests. I have benefited tremendously by being associated with him and his group.

I like to thank Professor Moustakas for his concern and encouragement throughout my graduate career and for his insights and valuable comments. I would also like to thank Professors Selim Unlu and Michael Yeung for the attention they have paid to timely reading of this manuscript. Thanks are also given to Professor Jan Smits for agreeing to act as the chairman of my thesis committee.

Without the cooperation and support of the technical staff of MIT Integrated Laboratory, this work could never have been accomplish. Thanks are given to Bernard Alamariu, Jim Bishop, Vicky Diadiuk, Brian Foley, Tom Takacs, Pat Varley and Joe Walsh. Many thanks to Paul Tierney and Dan Adams for their help with photolithography and for making the long hours spent in the lab fun. Thanks to B. Y. Kim and Professor Dim Lee Kwong of University of Texas at Austin for their help with the growth of oxynitride gates.

I would like to thank Professor Dimitri Antoniadis and Professor Martin Schmidt for allowing me access to their labs. Special thanks to Melanie Sherony, Keith Jackson and Tony Lochtefeld for helping with the set up of the CV system and to Lalitha Parameswaran for her help with the TMAH etching of polysilicon.

I would also like to thank to Dr. Norbert Strecker for his assistance with modeling the oxide mechanical system and his helpful discussion in developing the numerical code for oxidation.

Thanks also to many friends and officemates here at Boston University. Geng Bai, Soumya Banerjee, Marius Bunea, Srini Chakravarthi, Iuval Clejan, Alp Gencer, Brendon Murphy whose support and encouragements made life at BU a lot nicer. Special thanks to Marius Bunea for his modification of Lattice Monte Carlo simulator and to Alp Gencer for writing and supporting the partial differential solver DOPDEES. Without their help the modeling portion of this work could not have been possible.

A heartfelt thanks goes to my two old officemates and friends Dr. Anu Agarwal and Dr. Fred Wittel. Their patient explanations are responsible for much of my knowledge about IC processing.

I would like to dedicate this thesis to my parents for their love and support. I am deeply grateful to them for providing an appropriate learning environment and nourishing my scientific interests. Finally thanks to Octavio Marenzi for sharing all the ups and downs and moves across continents. I could not have accomplished any of this without his love and support.

Support of this work was provided by the Semiconductor Research Corporation through contract No. BJ-530-003.

DENSITY RELAXATION AND IMPURITY INCORPORATION IN THIN SILICON DIOXIDE FILMS AND THEIR EFFECTS ON BORON DIFFUSION

(Order No.)

MITRA NAVI
Boston University College of Engineering, 1998
Major Professor: Scott T. Dunham,
Associate Professor of Electrical Engineering

Abstract

Integrated circuit device geometries require precise control of thickness and electrical properties in thin gate dielectric. This work studies the evolution of excess density generated during thermal oxidation of silicon and the properties of the resulting oxide films. This work also investigates impurity incorporation in thin oxides and its effect on boron penetration leading to changes in threshold voltage.

Due to differences in molecular volume between silicon and SiO_2, the oxidation process results in the generation of stress near the Si/SiO_2 interface. This stress substantially reduces the diffusivity and solubility of oxidant species (e.g., O_2) in the oxide, modifying oxidation kinetics. To be able to model diffusion in the oxide as a function of stress, one is required to first model the stress generation and relaxation in the oxide. We have proposed a model that accounts for mechanical behavior of silicon dioxide. In the model, the newly created oxide is assumed to be highly compressed, relaxing as oxidation (or annealing) proceeds. The model was matched to both one and two-step oxidation kinetics to extract stress-dependent diffusivity and solubility for O_2 in SiO_2.

We also investigated the influence of oxide density on boron diffusion through thin gate dielectrics. Capacitor structures were fabricated by depositing polysilicon on top of 54–60Å oxide films grown at 800°C in dry O_2. A subset of these high density oxides (approximately 3–4% excess density) were then annealed at 1100°C, to relax the grown-in stress. Following ion implantation of boron into the polysilicon, the capacitor structures were annealed in an inert ambient at 950°C to allow boron penetration. Capacitance-voltage measurements revealed that boron penetration was greatly enhanced for the films that saw the high temperature relaxation anneal, leading to the conclusion that boron diffusion in SiO_2 is retarded in the presence of excess density.

This work also examines boron penetration from p^+ polysilicon through 50–70Å gate dielectrics following B or BF_2 implantation. Gate oxides were grown in N_2O/O_2 mixtures with average nitrogen contents varying from 0 to 1.4%. A series of capacitance-voltage measurements were used to determine the amount of boron penetration, and SIMS measurement were carried out to measure the depth profiles of incorporated nitrogen and fluorine. In addition, to better understand the role of fluorine, experiments were carried out to

investigate the redistribution of fluorine in the poly/SiO_2/Si system. A model was developed which accounts for the dependence of boron diffusion on composition and density.

Contents

List of Tables

List of Figures

Chapter 1

Introduction

1.1 Motivation

Thermally grown SiO_2 layers are an excellent natural insulator for silicon wafers. The most important use of such layers has been as a gate dielectric in metal-oxide-semiconductor (MOS) devices. This application also presents the most stringent requirements on film thickness control and on bulk and interface electrical properties.

As fabrication technology moves toward smaller device geometries, finer control of device spatial dimensions is required. Low-temperature processing ($< 900°C$) is important to limit diffusion of dopants in silicon. However, at these temperatures the property of the oxide films are found to be different than the oxide grown at higher temperatures. One such property is the stress generated during the growth of SiO_2 layers and its effect on the properties of the resulting film.

As gate dielectrics become thinner, dopant diffusion from the gate to the channel also becomes an increasingly important problem. Additionally, other impurities such as nitrogen are incorporated in the oxide films to improve the electrical and chemical properties [14]. Fluorine is introduced to the oxide when BF_2 is used as an implant source [15]. Large amounts of hydrogen are also incorporated when steam or hydrogen is present in the ambient [16]. The high solubility and low diffusivity of boron suggests that boron is tightly coupled into the oxide network. If this is true, the diffusion mechanism for boron (as well as other dopants) may be similar to that for the diffusion of silicon in the oxide structure. The data for silicon tracer diffusion exhibits an activation energy which falls in the range of those reported for viscous flow of oxide [17]. This suggests that silicon diffusion is closely correlated to viscous flow of the oxide. The correlation of changes in boron diffusion with impurities that alter oxide viscosity suggests that boron diffusion is also related to viscous flow. One of the focuses of this study is on the evolution of film density which can be viewed as a signature of stress and structural processes. The aim of this thesis is quantify the effect of oxide density and the incorporation of impurities which alter the oxide structure (N, F, H) on boron diffusion, and to develop quantitative models for these processes which can predict experimental behavior.

1.2 Thermal Oxidation and Relaxation

1.2.1 Oxidation Kinetics

Deal and Grove [18] were among the first to develop a linear-parabolic model for oxidation of silicon in both dry O_2 and steam ambients. They assumed that oxidation proceeds by the inward movement of a species of oxidant. The transported species must go through the following stages:

- It is transported from the bulk of the gas to the gas-SiO_2 interface where it reacts or is adsorbed.
- It is transported across the oxide film towards the Si-SiO_2 interface.
- It reacts with Si at the Si-SiO_2 interface to form SiO_2.

The assumption is made that oxidizing species diffuse rapidly across the oxide, so the oxidation process is in steady state and the flux of oxidants from each of the above steps are equal. The flux of oxidants from gas to outer surface of oxide is taken to be

$$F_1 = h\,(C^* - C_\mathrm{o}), \tag{1.1}$$

where h is a gas–phase transport coefficient, C_o is the concentration of oxidant at the outer surface of oxide at any given time and C^* is the equilibrium concentration of oxidant in the oxide. The equilibrium concentration of oxidant is related to partial pressure of the oxidant by

$$C^* = Kp, \tag{1.2}$$

where K is Henry's constant for the oxidant species.

The flux of oxidant across the oxide is assumed to be given by Fick's law,

$$F_2 = -D_\mathrm{eff}\left(\frac{dC}{dx}\right), \tag{1.3}$$

where D_eff is the effective diffusion coefficient and dC/dx is the concentration gradient of oxidizing species across the oxide.

Finally, the flux of oxidizing species due to reaction at the interface is given by

$$F_3 = k_i C_i. \tag{1.4}$$

where C_i is the interface concentration of oxidizing species and k_i is the oxidation reaction rate constant. Setting these fluxes equal and solving for oxidation rate we have,

$$\frac{\partial x_\mathrm{o}}{\partial t} = \frac{F}{N_1} = \frac{k_i C^*}{N_1\,(1 + k_i/h + k_i x_\mathrm{o}/D_\mathrm{eff})}, \tag{1.5}$$

where N_1 is the number of oxidant molecules in a unit volume of oxide layer. Using the initial condition of $x_\mathrm{o} = x_\mathrm{i}$ at t=0, and integrating above equation gives,

$$\frac{{x_o}^2 - x_i^2}{A} + \frac{x_o - x_i}{B/A} = t, \tag{1.6}$$

or

$${x_o}^2 + Ax_o = Bt + x_i^2 + Ax_i, \tag{1.7}$$

which can be rewritten in the form

$${x_o}^2 + Ax_o = B(t + \tau), \tag{1.8}$$

where

$$A = 2D_{\text{eff}}\left(1/k_i + 1/h\right), \tag{1.9}$$

$$B = 2D_{\text{eff}}C^*/N_1, \tag{1.10}$$

and

$$\tau = x_i\left(x_i + A/B\right), \tag{1.11}$$

Solving the quadratic Equation of 1.8

$$x_o = \frac{A}{2}\left[\left(1 + \frac{t+\tau}{A^2/4B}\right)^{1/2} - 1\right], \tag{1.12}$$

which gives the oxide thickness as a function of time. At relatively large times ($t >> A^2/4B$)

$${x_o}^2 \cong Bt, \tag{1.13}$$

which is the well known parabolic oxidation law for relatively long times.

The Deal-Grove model is known to fit experimental oxidation data for a wide range of temperatures. However, as integrated circuit technology requires smaller devices and lower temperature processing the accuracy of the model and its explanation of oxide growth were found to be insufficient. The issue is prediction of thin oxides, the experimental growth rates deviates significantly from the linear-parabolic dependence. The experiments a show a high initial oxidation rate which can not be explained by Deal-Grove model.

New technologies require better control of thinner films as well as higher dimensional geometries. It is therefore apparent that better physical models must be developed to include the role of interface and surface reactions and diffusion and solubility of oxidant. In addition, the effect of the stress, which is known [4] to effect the oxidation parameters must be accounted for.

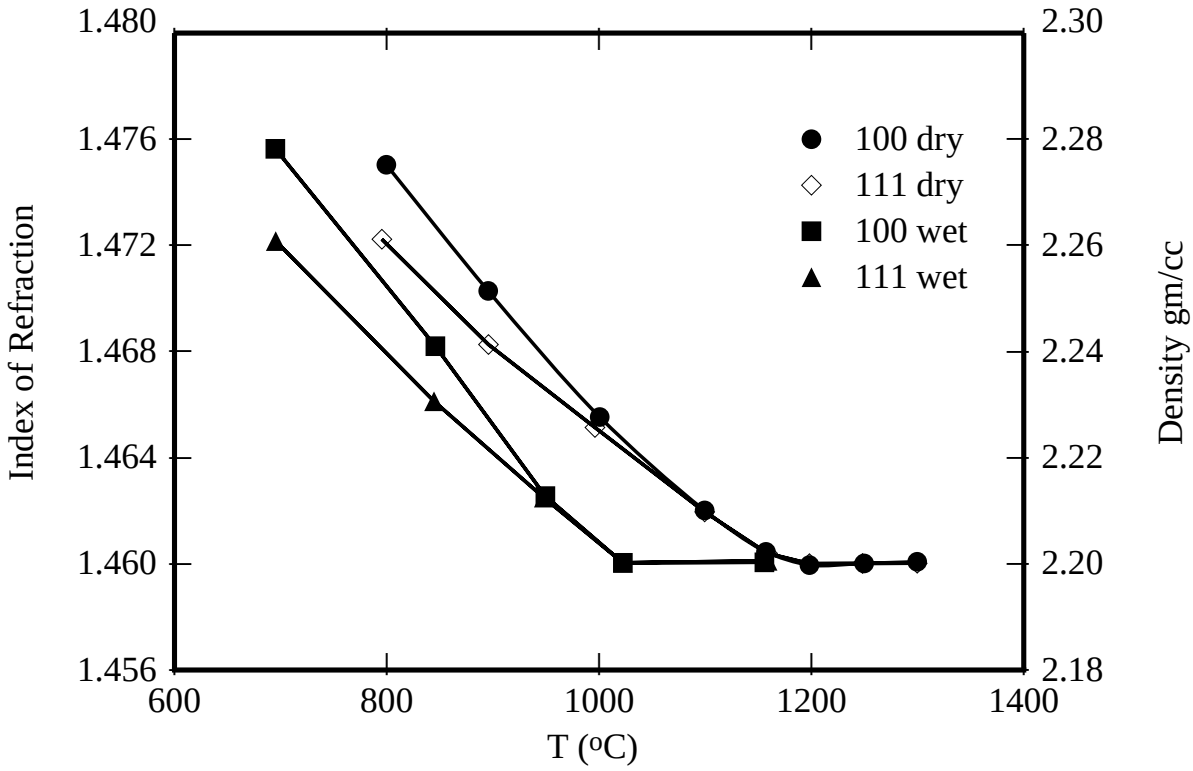

Figure 1.1: Refractive index versus growth temperature for wet [1] and dry [2] oxides and density [3] for dry oxides on Si.

1.2.2 Evolution of Stress During Oxidation

Due to the volume expansion during oxidation, large stresses exist in the oxide. Incorporation of oxygen in the oxide network at the interface is accompanied by 30% strain in each linear direction. This demand for extra space cannot generally be satisfied,
except at high temperatures. The network cannot rearrange fast enough by viscous flow, therefore the resulting film maintains substantial residual stress and strain [4].

EerNisse [19] showed that for growth temperatures above 900°C, the curvature of oxidizing Si wafer remains constant during growth, below 950°C the Si curvature changes with thickness of grown SiO_2. He reported that below 950°C the curvature changes are related to compressive stress in oxide, above 950°C however, the viscosity is low enough that the oxide could grow stress-free.

It is also known [1] that film refractive index increases with decreasing growth temperature. For both wet and dry oxides, there is a well defined breakpoint in temperature, above which the refractive index reaches a minimum value and does not change any further (see Figure 1.1). The breakpoints are at 1150–1200°C for

dry oxidation and at $\sim$1000°C for wet oxidations. The minimum refractive index value is found to be the same for both wet and dry oxidations. This minimum value corresponds to refractive index of pure fused quartz [2] which are representative of a "fully–relaxed" oxides.

Landsberger [20] used the results from index of refraction studies [1] to investigate the inert annealing of low temperature oxides. He grew oxides at 800°C which he then annealed in inert ambient at various temperatures. He observed that the refractive index of 800°C oxide dropped from its original 1.472 to 1.460. This reduction was accompanied by oxide swelling of $\sim$3% (see Figure 1.2).

Analysis of such experiments can give information about the mechanical characteristics of SiO_2 film. By studying stress and strain relaxation one can hope to explain the annealing behavior of SiO_2 films. Furthermore, relaxation experiments in conjunction with the two step oxidation experiments [5] can be used to model the dry thermal oxidation and the rapid initial oxidation regime by including the dependence of oxidation parameters on time-dependent stress evolution in oxide.

1.3 Incorporated Impurities in Oxide

1.3.1 Nitrogen

The growth of high quality gate oxide film has become important for submicron integrated circuits device technology. However, there are many technological as well as reliability issues associated with very thin oxides [21, 22]. Thermal nitridation of silicon dioxide is an alternative approach for growing very thin gate dielectrics. The motivation for using oxynitrides is that incorporated nitrogen strengthens the gate dielectric, decreases trapping rates, increases charge-to-breakdown and increases hot

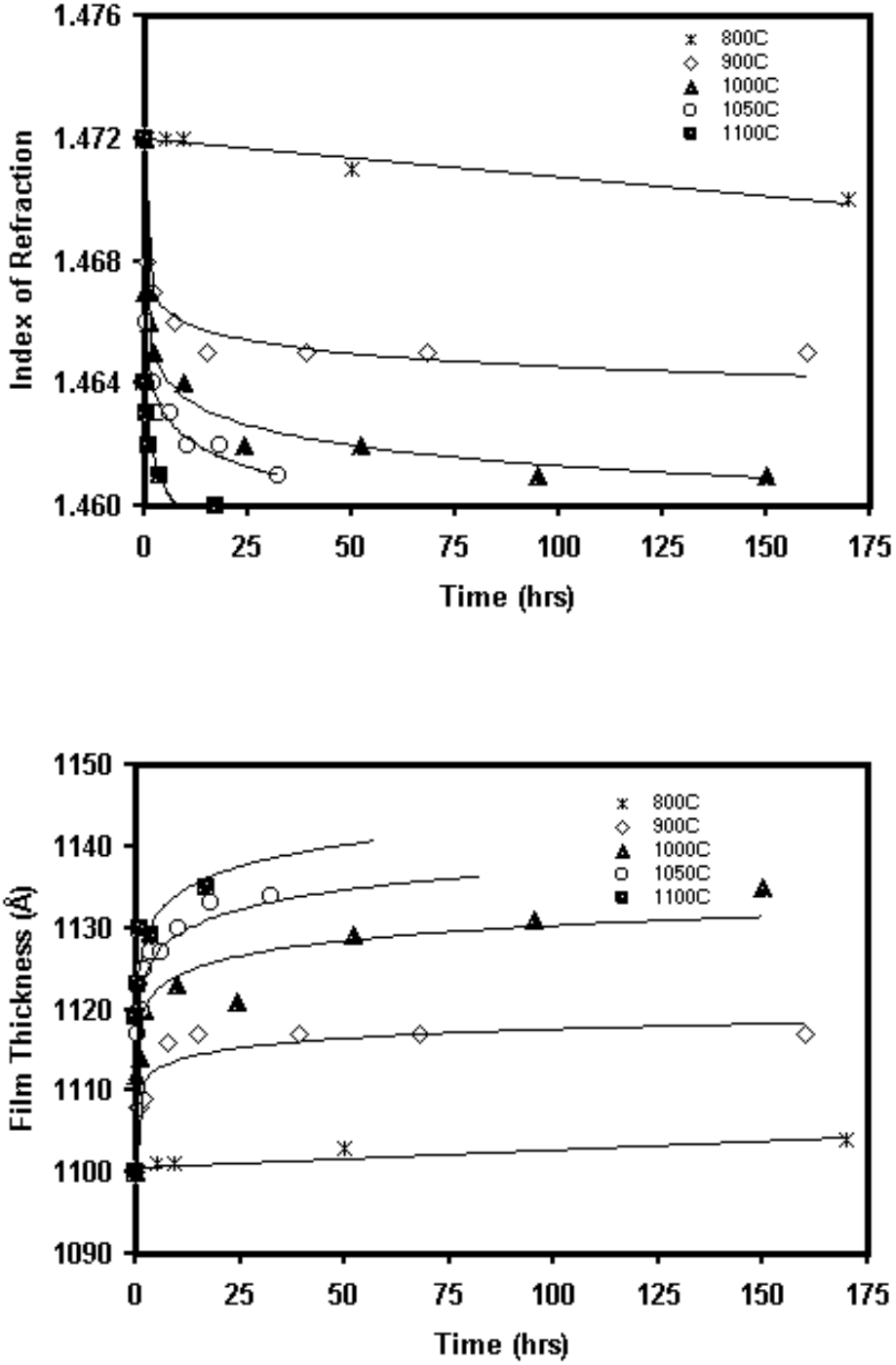

Figure 1.2: Refractive index N_{ox} and thickness X_{ox} as function of anneal time for initially 800°C, (111), dry-grown SiO_2 films on Si. Data from Landsberger *et al.* [4]

carrier immunity [22, 23, 24]. Among the approaches for nitrogen incorporation in oxide, NH_3 nitridation of SiO_2 and oxidation of Si in nitrous oxide (N_2O) or nitric oxide (NO) ambients are the most common ones [22, 25, 26]. Although NH_3 nitrided thermal oxides exhibit superior gate dielectrics due to large nitrogen incorporation in the oxynitride, these dielectric films suffer from hydrogen related electron trappings. Oxynitrides grown in N_2O and NO gas ambients, however, show improved electrical characteristics [27, 22] as well as providing good barrier for impurity diffusion [28].

Although all above methods result in incorporation of nitrogen in the oxide, the distribution of nitrogen is distinctively different in each case. All methods show a nitrogen pile up near the interface [29] however, N_2O and NO oxides show lower nitrogen concentration than reoxidized NH_3-nitrided SiO_2. NO oxynitrides provide much tighter N distribution at the interface [30]. This has been attributed to the fact that NO oxynitrides grow as a result of NO reaction with SiO_2/Si as compared to N_2O oxynitride growth where NO and O_2 reaction take place in parallel [30]. It is known [23] that the structure of pure silicate glass is modified when nitrogen is present in the network. The trivalent nitrogen atoms are linked to three silicon atoms which reduce the open ring structure of oxide and increases crosslinks (see Fig 1.3). This transformation makes the oxynitride more viscous, denser, stronger and more refractory [31]. XPS studies of oxides grown in NO ambient do indeed show an intense and clearly defined N (1s) peak with a binding energy close to the measured binding energy value of Si$\equiv$N bonds in Si_3N_4 [30]. In N_2O grown oxynitrides however the dominate bonding state is the $\equiv$Si-N-Si$\equiv$, where nitrogen atoms are bonded to only two Si atoms with remaining bond being a dangling bond [32, 30].

1.3.2 Fluorine

In recent years, p^+-polysilicon has been proposed to substitute for conventional n^+-polysilicon as the gate material of p-channel MOSFETS to convert buried channel to surface channel operation. The p^+-gates are typically fabricated by implanting B or BF_2 into intrinsic polysilicon. The role of fluorine in the oxidation of silicon has been also a subject of considerable interest. The incorporation of fluorine enhances oxide

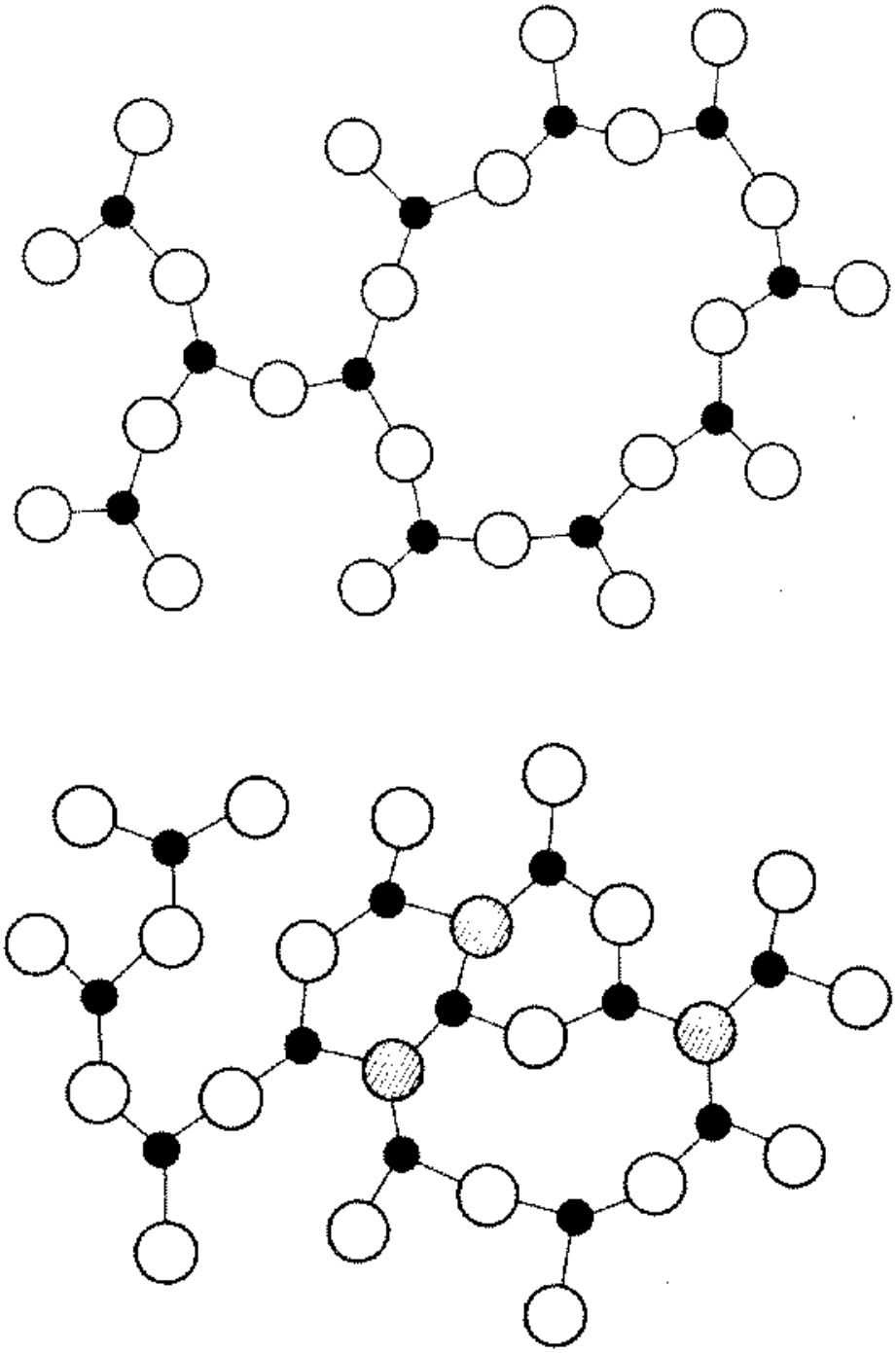

Figure 1.3: Comparison of oxide and oxynitride for pure silicate glass. Dark circles denote silicon, large open circles denote oxygen and the hatched circle are the incorporated nitrogen atoms in the silicate glass structure.

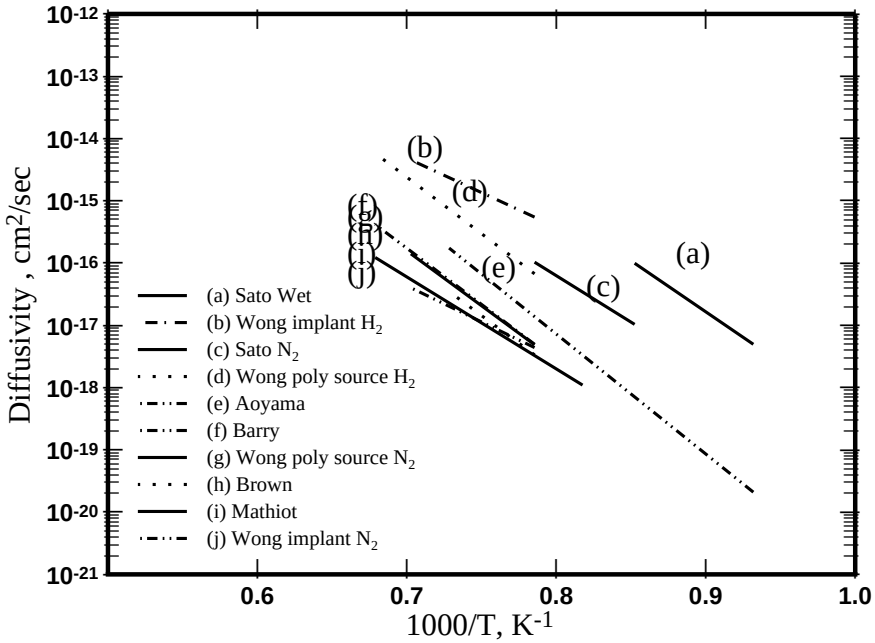

Figure 1.4: Boron diffusivity SiO_2 as a function of temperature.

growth, reduces oxidation induced stalking faults and retards oxidation enhanced diffusion [33].

It has been shown that when appropriate amounts of fluorine are introduced into the oxide, stress relaxation of the dielectric is observed [34]. The mechanism by which fluorine causes stress relaxation, is related to fluorine-induced oxide density reduction and opening up of the oxide structure due to formation of Si-F bonds. Indeed XPS studies of oxides grown in NF_3 ambient show that fluorine atoms in the oxide primarily bond to silicon and not to oxygen [35]. The new configuration of oxide is more relaxed which gives rise to higher resistance to radiation and hot-carrier damage [36].

1.3.3 Hydrogen

Although hydrogen in the form of steam has been used intentionally during thermal oxidation to increase oxidation rates very often it is also incorporated unintentionally into SiO_2 films. Like fluorine, hydrogen passivates the silicon or oxygen dangling bonds in SiO_2 structure. It is also known that hydrogen passivates certain defects in the oxide [37, 38]. This passivation also increases the number of non-bridging oxygens which in turn reduces the viscosity of the film substantially [39].

1.3.4 Boron Diffusion in Oxide

One of the difficulties associated with the scaling of CMOS (complementary metal-oxide-semiconductor) processes is the scaling of gate dielectric. The concern is the diffusion of boron through the gate oxide. Boron has a high solubility and low diffusivity in oxide which suggests that it is tightly coupled into the oxide network. However, it is known [11, 9, 28] that for thin oxides ($<$80Å) boron penetration from p^+-polysilicon gate can cause fluctuation in flat band voltage (V_{FB}) [40]. This is accompanied by increase in electron charge trapping and inverse subthreshold slope [41].

To be able to control diffusion of boron in PMOS devices, many workers have tried to characterize boron diffusion in oxide. The result is a wide range of diffusion coefficients for boron in SiO_2. Figure 1.4 and Table 1.1 summarize the existing data in the literature. The data shows a wide spread over the temperature range of 800-1200°C.

The discrepancy can largely be attributed to the experimental approach. The diffusivity of boron can be modified by many factors such as annealing ambient, dopant effects and oxide structure. For example, the presence of hydrogen in the ambient can passivate dangling bonds in the SiO_2 network and therefore make boron more mobile in the SiO_2. Increased boron diffusivity is observed when fluorine is introduced in the oxide [11]. In contrast nitridation of SiO_2 layer is known [28, 45] to reduce boron diffusivity in the SiO_2. Injection of silicon interstitials in the oxide also been proposed to decrease boron diffusivity [10].

1.4 Organization

This thesis is organized in the following manner. Chapter 2 presents the physical model used for the simulation of oxidation. Both relaxation and oxidation models are presented. The relaxation as well as two step oxidation experiments performed by Landsberger are used for testing and extracting the model parameters. Also described is the one dimensional oxidation simulator which solves the mechanical equations as well as the transport equations for oxidizing species.

Chapter 3 describes experimental work on the dependence of boron diffusion on oxide density. It takes advantage of the built-in stress in planar films, which can be adjusted by adjusting the oxidation as well as the annealing temperature, to influence boron diffusion in oxide.

Chapter 4 describes the effect of nitrogen incorporation on boron diffusion in oxide. Several experimental procedures were designed to characterize this behavior. Gate dielectrics with different amount of incorporated nitrogen were fabricated and boron diffusion through these films are studied. This chapter also describes the result of lattice Monte Carlo calculations used to determine the function dependence of boron diffusivity on the amount of incorporated nitrogen.

Chapter 5 illustrates the effect of incorporated Fluorine on boron diffusion. Experimental results of fluorine redistribution in poly/oxide/Si is presented and models describing the observed phenomena is described.

Finally, Chapter 6 summarizes the contributions of this study and presents some recommendation for future work.

Diffusivity of B in Oxide						
Reference	D_o (cm^2/min)	Q (eV)	Initial Oxide (°C, nm)	Source	Implant (cm^2, keV)	Ambient (°C)
Wong [15] (SIMS)	3.5e-4	3.5	800, 12.5 steam	poly, 300nm	5e15, 20	N_2 1000-1150
Wong [15]	1.2e-2	3.6	800, 12.5 steam	poly, 300nm	5e15, 20	H_2 1000-1150
Wong [15]	5.6e-9	2.3	950, 500 steam	-	5e15, 20	N_2 1000-1150
Wong [15]	2.8e-7	2.2	950, 500 steam	-	5e15, 20	H_2 1000-1150
Mathiot [28] (SRP)	1.3e-6	2.93	900, 10 O_2	poly, 380nm	3e15, 30	N_2 970-1200
Sato [42] (CV)	5.4e-5	2.96	800, 5 O_2	poly, 380nm	1e16, 35	N_2 900, 1000
Sato [42]	9.1e-3	3.25	800, 5 O_2	poly, 500nm	1e16, 35	steam 800, 900
Aoyama [11] (SIMS)	1.83e-2	3.82	1000, 6 O_2	poly, 320nm	1e16, 20	? 800-1100
Brown [43] (4-p. probe)	3.16e-4	3.53	-	Borosil.	-	? 1000-1100
Barry [44] (4-p. probe)	7.38e-4	5.58	-	Borosil.	-	N_2 1000-1100

Table 1.1: Processing steps and extracted diffusivities for B diffusion through SiO_2

Chapter 2

Stress Generation and Relaxation

2.1 Introduction

Thermal oxidation of silicon is an essential step in VLSI technology. Modeling the process is necessary for predicting the oxide shape and thickness. Due to the volume expansion during oxidation, large stresses exist in the oxide [46]. Measurements of oxide refractive index show that the stress increases for oxides grown at lower temperatures [1, 47], in agreement with the observation that annealing of oxides grown at low temperature causes the films to swell [4, 48]. The reduced oxide thickness grown on silicon corners indicates that stress can reduce the growth coefficients [49] and experiments indicate that the diffusivity as well as the solubility of oxidizing species are likely to be influenced by this stress [50]. Fargeix *et al.* [51] reported that local compressive stress exists in the SiO_2 which is at its maximum at the Si-SiO_2 interface and decreases monotonically towards the free surface of the oxide. They suggested that molecular diffusivity in such a stressed film is therefore lower than the same film when unstressed.

Oxide layers with various stress levels can be generated by varying the growth temperatures. Thus, the dependence of growth rate parameters on stress in the oxide can be studied by comparing the additional thickness of the oxide grown underneath differently stressed layers. The two-step oxidation experiments such as those performed by Landsberger *et al.* [5] can therefore be used to understand history effects in thermal oxide and to quantify the dependence of growth parameters on generated stress during oxidation.

Isolation technologies such as local oxidation of silicon (LOCOS), buried oxide (BOX) and deep trench have been modeled by a number of workers [52, 53]. In many of these analyses, fully viscoelastic models have been developed to predict the oxide shape by including the dependence of oxidation parameters on stress. However, such models which consider stress-dependent oxidation in 2 and 3D structures generally ignore the higher density of oxide produced at lower temperatures even in planar structures [50, 52, 53, 39]. Thus the baseline for “stress free” diffusivity and solubility used in these models are actually the values at the stresses typical of oxides grown at those temperatures, which relaxation and two-step oxidation experiments [4, 54, 3] clearly reveal as very different from the true “stress free” values.

In this work, we develop a model for stress generation/relaxation and its effect on oxidation kinetics which includes the initial formation of a high density oxide. Analysis of oxide relaxation experiments are used to extract the mechanical characteristics of SiO_2 films. The model is then applied to one [7] and two-step oxidation kinetics [5] and stress-dependent oxidant diffusivity and solubility are extracted.

2.2 Modeling

To be able to accurately predict oxide thickness as a function of time, one must first establish the mechanical models for oxidation. Depending on temperature, one can expect the oxide to behave as a solid or fluid. A number of models have been proposed to describe the behavior of oxide [13, 55, 56]. In this work, a compressible viscous model, which represents a distributed (spatially varying) version of the model used by Rafferty *et al.* [13] is proposed to account for the behavior of SiO_2.

To construct the model, we first express the principle of conservation of mass in the oxide as:

$$\frac{\partial \rho}{\partial t} + \frac{\partial (\rho V)}{\partial x} = 0, \tag{2.1}$$

where ρ is the mass density of the material and V is the velocity. Next, the momentum balance for steady flow is described by the Navier-Stokes equation as:

$$\rho\left(\frac{\partial V}{\partial t} + V\frac{\partial V}{\partial x}\right) = \frac{\partial \sigma}{\partial x}, \tag{2.2}$$

where σ denotes the stress. Finally the material law for a compressible viscous material is [57]:

$$\sigma = -P + (\lambda + 2\mu)\frac{\partial V}{\partial x}, \tag{2.3}$$

where P is the pressure, λ is the Lame constant and μ is the viscosity. Furthermore, the pressure P is related to mass density by:

$$P = P_0 + P_1\frac{\rho - \rho_1}{\rho_1}, \tag{2.4}$$

where P_0 is the atmospheric pressure, P_1 is the Young modulus of SiO_2 [58], and ρ_1 is the equilibrium oxide density (~ 2.22 gr/cm^3). In this model, the viscosity (μ) is allowed to depend on stress such that [39]:

$$\mu = \mu_0\,\frac{\sigma/\sigma_c}{\sinh(\sigma/\sigma_c)}. \tag{2.5}$$

Next, we have to account for the oxidant diffusion through the oxide and reaction at the interface. As mentioned previously, stress generated during oxidation can affect the diffusivity (D) and solubility (C^*) of the oxidant species. The diffusivity and solubility can be written in the form [50]:

$$D = D_0 \exp\frac{(-PV_D)}{kT}, \tag{2.6}$$

$$C^* = C_0^* \exp\frac{(-PV_C)}{kT} \tag{2.7}$$

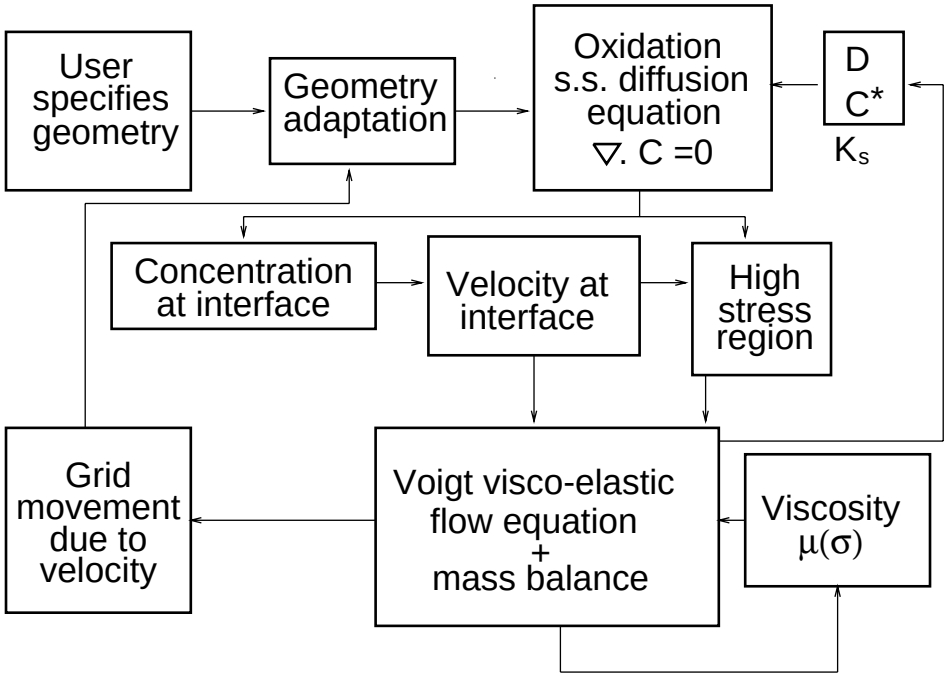

Figure 2.1: An overview of the 1D finite element solution method

where V_D and V_C are the activation volume for diffusion and solubility respectably. For the 1D systems considered in this work, there is no normal stress so the interface reaction rate k_s is fixed.

Incorporating the above assumptions, one can represent the transport equation for oxidizing species as:

$$\frac{\partial}{\partial x} DC^* \frac{\partial C/C^*}{\partial x} = 0, \tag{2.8}$$

where C is the concentration and D is the diffusion constant of the oxidizing species. The above equation is assumed to be in steady state and subject to boundary conditions:

$$DC^* \frac{\partial C/C^*}{\partial x} = k_s C, \tag{2.9}$$

at the Si/SiO_2 interface ($x = 0$) and

$$DC^* \frac{\partial C/C^*}{\partial x} = h(C - C^*), \tag{2.10}$$

at the SiO_2/gas interface ($x = x_o$) where h is the gas-phase transport coefficient. The solution to Eq. 2.8 provides the boundary conditions for the velocity. However, instead of generating a large volume of unstressed oxide, as is most commonly done [7, 18], we assume that a region of high stress is created with the same volume as the silicon consumed [59] and density

$$\rho = m_{ox} C_{si}, \tag{2.11}$$

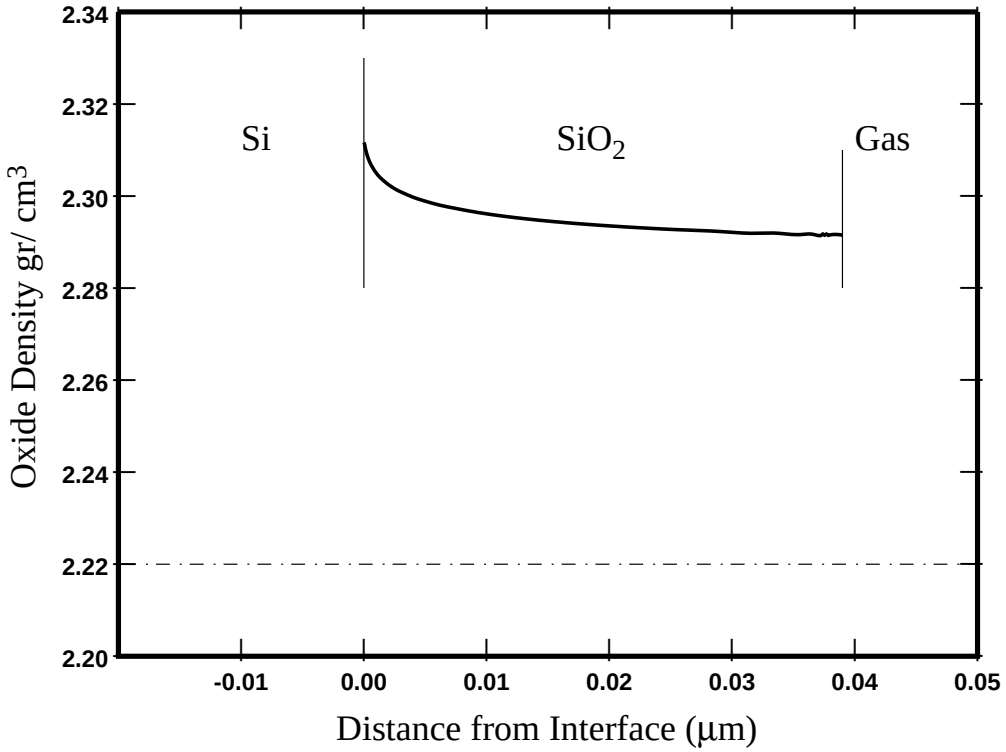

Figure 2.2: Simulated density distribution for an oxide film grown at 800°C in dry O_2 on ⟨111⟩ silicon. The equilibrium oxide density is also displayed as reference.

where m_{ox} is the molecular mass of the oxide and C_{si} is the atom concentration of silicon (as opposed to SiO_2). This high density region is relaxed by solving the coupled partial differential equation of mass and momentum balance, which also contributes to the growth of the oxide.

It can be noted that the equations for mass (Eq. 2.1) and momentum balance (Eq. 2.2) are two coupled nonlinear partial differential equations. These equations cannot easily be solved by analytical techniques. Therefore numerical techniques are essential. A one dimensional finite element discretization of the above model has been implemented. Figure 2.1 shows the numerical computation flow chart for a typical time step. Appendix A describes the details of this implementation.

2.3 Results and Discussion

Figure 2.2 shows the result of the above model for a 500 min oxidation at 800°C. The high stress generated at the interface $\rho = m_{ox}C_{si}$ ($\sim$ 4.99 gr/cm^3) relaxes almost immediately to a value of about 2.31 gr/cm^3 at 800°C. This value is calculated from the amount of relaxation in the time it takes to grow half a monolayer of

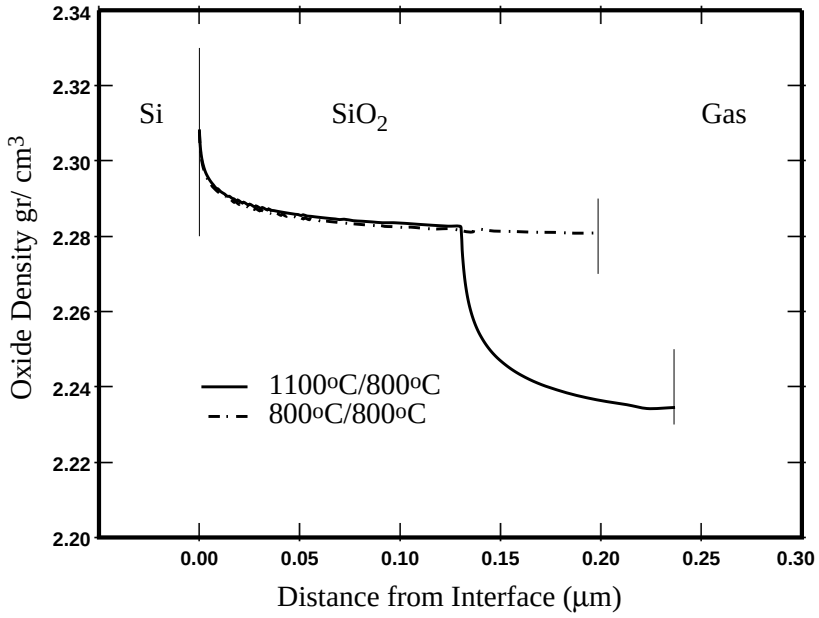

Figure 2.3: Simulated density distribution for oxides grown at 1100 and 800°C to a thickness of 1070Å and subsequently reoxidized at 800°C for 65h.

oxide. The rapid relaxation is due to the strongly nonlinear behavior of viscosity at high stresses. For stress in the oxide greater than the critical stress σ_c, the viscosity reduces, causing the oxide to flow much more readily. The non-uniformity of the density profile in the oxide is due to the fact that relaxation continues for the already formed SiO_2, as this oxide is continuously exposed to the oxide growth temperature. This is in agreement with the *in situ* SiO_2 stress measurements as a function of oxide thickness reported by Kobeda *et al.* [46].

2.3.1 $\langle 111 \rangle$ Data

Using viscosity in unstressed SiO_2 (μ_0) from data on bulk silica [60], the model was matched to oxide relaxation data of Landsberger *et al.* [5] to extract the parameter σ_c. The relaxation experiments were as follows. Dry oxide films grown on lightly doped *p*-type Si $\langle 111 \rangle$ wafers at 800°C were annealed in inert ambients. The annealing process caused the oxide to swell by $\sim$3% of its as-grown thickness. Figure 2.4 shows the fit of the model to this data and Table 2.1 shows the extracted σ_c for various temperatures. Also shown are the values of σ_c extracted by Rafferty *et al.* [13]. The difference can be attributed primarily to the fact that Rafferty used not only σ_c but also the value of viscosity for unstressed oxides as fitting parameters finding a lower bulk viscosity. In addition, the model used in this work considers the variation of stress within the film, rather than assuming a homogeneous film as in the model used by Rafferty *et al.* [13]. This allows the

Extracted Critical Stress					
$\sigma_c(10^9$ dynes/cm$^2)$	800°C	900°C	1000°C	1050°C	1100°C
This work	0.94	0.94	1.49	2.17	3.58
Rafferty [13]	0.43	0.43	0.66	0.82	0.88

Table 2.1: Extracted value of σ_c for various temperatures for this work and from Rafferty *et al.* [13].

application of the same model to oxidation kinetics through the dependence of diffusivity and solubility on local excess density in the SiO_2.

Once the mechanical parameters were established, the model was further matched to two-step oxidation experiments [5] and standard one-step oxidation kinetics [6], optimizing the stress dependent diffusivity and solubility parameters. The solubility of O_2 at 1 atm in unstressed oxide is taken from permeation experiments for vitreous silica ($C_0^* = 1.1\times10^{16}$ exp$(0.17/kT)$ cm^{-3} [61]) and the activation volume for diffusion and solubility are assumed equal ($V_C = V_D$). In two-step oxidation experiments [5],
the amount of oxide grown in the second step depends greatly on the growth temperature used in the first step. This is accounted for by the dependence of the diffusivity and solubility on the stress distribution in the oxide. Figure 2.3 shows the simulated density distributions in oxides grown to a thickness of 1070Å at either 1100 or 800°C and then oxidized at 800°C for 65 hours. As is seen experimentally [5], the films which are grown with an initial higher temperature oxidation experience an enhanced oxidation rate for the second step. The reasons for this behavior are illustrated in Figure 2.3, where the lower density of oxide grown at higher temperature leads to higher oxidant solubility and diffusivity.

The model accounts for both two-step and one-step oxidation kinetics data over a temperature range of $800-1180$°C as illustrated in Figure 2.5. The three curves which start with an initial oxide thickness of 1070Å correspond to the two-step oxidation experiments [5]. Note that thermal history effects are due to the greater oxide relaxation for film grown at higher temperatures. The activation volumes ($V_D = V_C$) and the stress-free values for the diffusivity and interface reaction rate are fitted to both one-step as well as two-step oxidation kinetics data. Table 2.2 provides a summary of the parameters used. Figures 2.6 and 2.7 show the extracted values of unstressed diffusivity (D_0) and interface reaction rate (k_s) for dry oxidation of $\langle 111\rangle$ Si. Also plotted are the values of D and k_s calculated from the results of Massoud *et al.* [7] and Landsberger *et al.* [5] using $C_0^* = 1.1\times10^{16}$exp$(0.17/kT)$ cm^{-3} [61]. It can be noted that the optimized values of the diffusivity and interface reaction rate are larger than values reported by previously [7, 18]. This difference is attributed to the fact that effective values extracted for these parameters are generally reduced due to the presence of stress in the oxide, while values for these parameters extracted from our model reflect the diffusivity and reaction rate for an unstressed oxide.

At higher temperatures, bulk density approaches the equilibrium density and effective parameters might be expected to approach the values in unstressed oxide. Figure 2.6 depicts this trend: At higher temperatures,

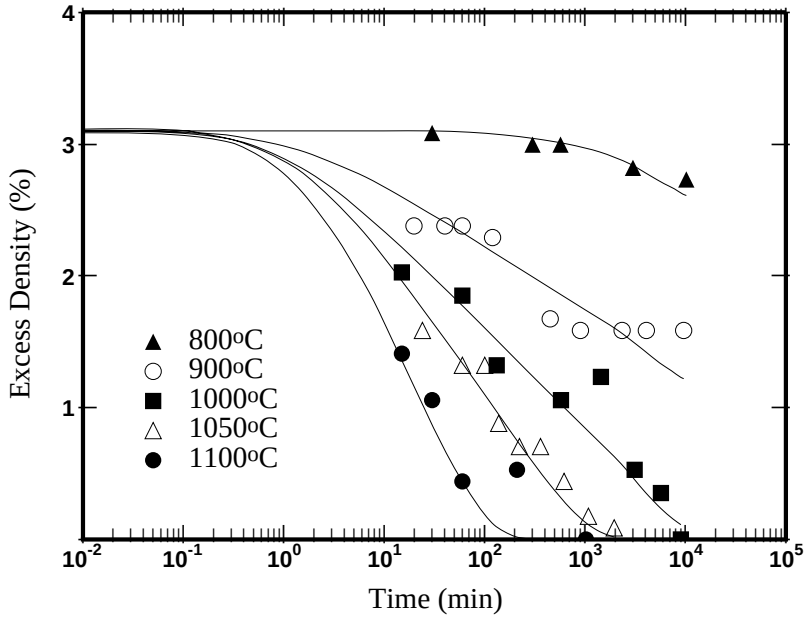

Figure 2.4: Excess oxide density versus annealing time over a range of temperatures. Data from Landsberger *et al.* [4]. Note that the model predicts the original excess density as well as the relaxation kinetics.

the diffusivity from the above model approaches reported effective diffusivities. This is further supported by the fact that the activation energy for D_0 (0.96 eV) is similar to that reported for high temperature oxidation [3, 18]. The diffusivity values reported in this work are very similar to the values reported by Landsberger *et al.* [5] for 1180°C oxides that were reoxidized at lower temperatures (see Figure 2.6) consistent with the fact that oxides grown at such a high temperature are nearly fully relaxed.

In contrast to diffusivity the extracted reaction rates do not approach the reported effective values even at high temperatures (see Figure 2.7). There are two factors that account for this behavior. The first factor is the effect of stress at the interface on solubility of oxidizing species. Although the stress at the interface reduces at high temperatures, its temperature dependence is relatively weak due to the nonlinear viscosity. This results in a reduced C^* at the interface even for higher temperatures, which reduces the concentration of oxidizing species at the interface. To be able to account for oxidation kinetics, the reaction rate must then be increased. Secondly

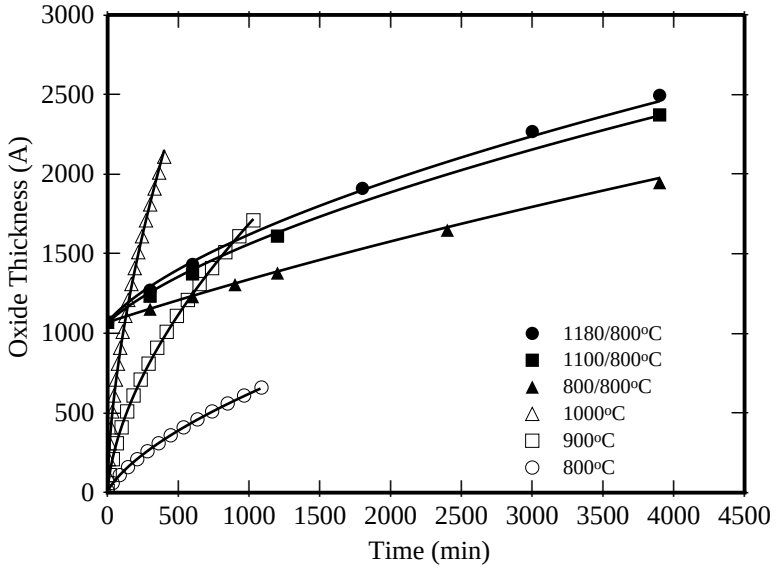

Figure 2.5: Comparison of model simulation to two-step [5] and one-step oxidation kinetics data [6]. Note faster growth at 800°C from initial 1070Å thickness for oxides initially grown at higher temperatures.

Model Parameters			
Parameter Description	Activation Energy	Pre-exponential	Source
Diffusivity of O_2 in Unstressed SiO_2 (D_0)	0.96 (eV)	4.6×10^{5} ($\mu m^2/min$)	Fitting Parameter
Interface reaction rate in unstressed SiO_2 (k_s)	2.84 (eV)	6×10^{15} ($\mu m/min$)	Fitting Parameter
Activation volume ($V_C = V_D$)	–	$13.8Å^3$	Fitting Parameter
Solid solubility of O_2 in unstressed SiO_2 (C^*)	-0.17(eV)	1.1×10^{16} (cm^{-3})	Permeation Experiments [61]
Viscosity of unstressed SiO_2 (μ_0)	-7.045(eV)	3.1×10^{-13} (poise)	Bulk silica [60]
Bulk Modulus of SiO_2 (P_1)	–	4.5×10^{11} (dynes/cm^2)	From Spinner [58]

Table 2.2: Summary of model parameters used in this work

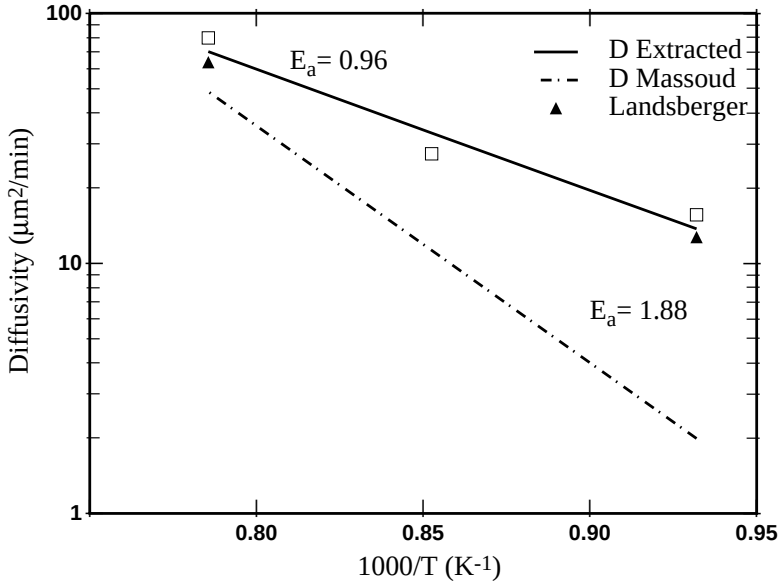

Figure 2.6: Extracted values of O_2 diffusivity in unstressed SiO_2 as function of temperature and comparison to values based on work by Massoud *et al.* [7] and Landsberger *et al.* [5].

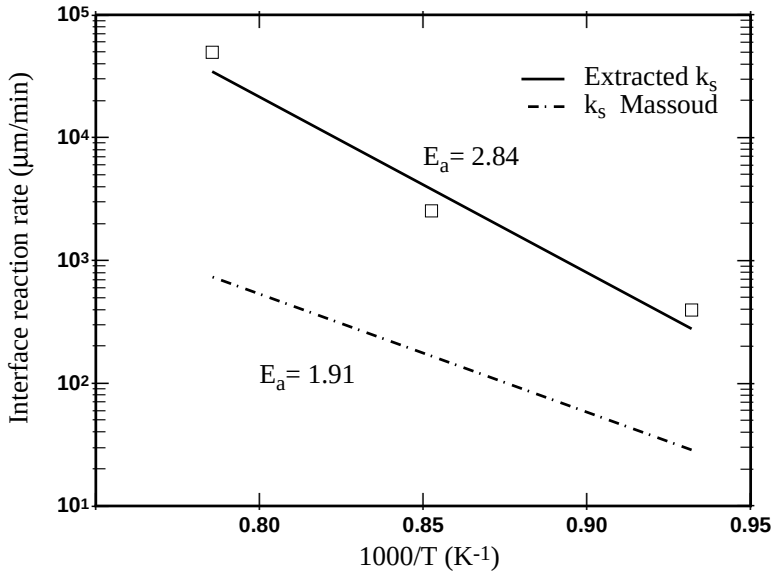

Figure 2.7: Extracted interface reaction rate values for O_2 as function of temperature for oxidation of ⟨111⟩ silicon and comparison to values calculated from model without stress dependent oxidation [7].

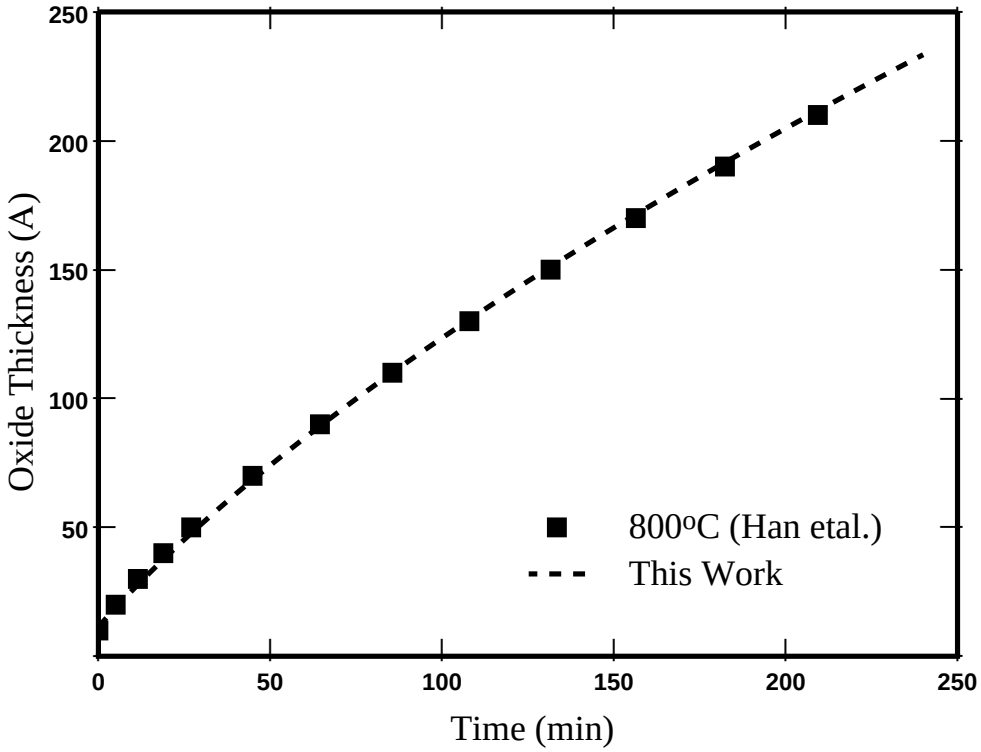

Figure 2.8: Comparison of model to oxidation kinetics in the thin regime from two-stream model of Han [6] fitted to data of Massoud [7].

the region of maximum stress near the interface reduces the diffusivity considerably. Again this reduces the availability of oxidizing species, requiring a larger reaction rate. Figure 2.8 shows a comparison between thin oxide kinetics of Massoud [6] and the model of stress-dependent oxidation developed in this work. Although the model was developed primarily to account for relaxation and two-step oxidation, it also does a very good job predicting behavior in the thin oxide regime. The explanation for the initially rapid oxidation predicted by the model is that for thicker oxides, a compressed region near the interface is established, with a thickness that varies only slowly as the film grows. For moderate oxide thicknesses, it is the combination of the slower diffusion through this interface layer and the interface reaction which limits the growth rate. For very thin films, this layer has not yet been fully established and thus the initial growth rate is higher than the linear growth rate that would be extracted by including only thicker films.

2.3.2 $\langle 100 \rangle$ Data

We also applied the model to oxide relaxation data for $\langle 100 \rangle$ silicon wafers reported by Taniguchi *et al.* [8] (Figure 2.9). In these experiments oxides, of 1020Å with reported refractive index of 1.4687 were grown

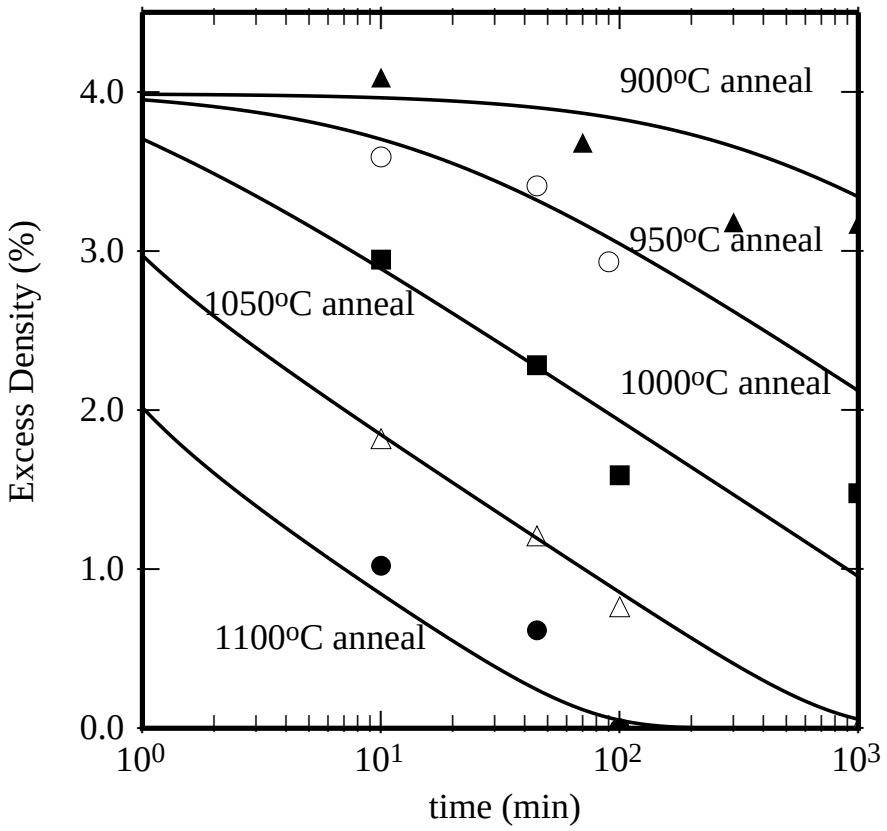

Figure 2.9: Excess oxide density versus annealing time over a range of temperatures. Data from Taniguchi *et al.* [8]. Note that the model predicts the original excess density as well as the relaxation kinetics.

in dry oxygen on ⟨100⟩ single-crystalline silicon at 900°C for 14 h. After the oxidation, the wafers were annealed in an argon gas ambient at various temperatures for 10–1000 min to relax the oxide. The changes in the refractive index and oxide thickness were measured using ellipsometry after the thermal annealing. We were able to match the above data with a single σ_c value of 1.8×10^9 (dynes/cm^2) for all temperatures.

2.4 Conclusions

A compressible viscous model has been developed to account for the oxidation of silicon. In this model, a highly compressed oxide is created at the Si/SiO_2 interface and is relaxed by solving the equations for mass and momentum balance in the bulk of the oxide. A 1D oxidation code has been developed to solve these equations and mechanical parameters were optimized to relaxation data. The model was further extended to include the stress dependence of oxidation rate parameters. These parameters were fit to oxidation kinetics reported in the literature. A stress-dependent diffusivity (D) and solid solubility (C) have been extracted for ⟨111⟩ Si. The model accounts for the oxide relaxation behavior as well as thermal history effects on oxidation

kinetics and thin oxide kinetics.

Once the stress dependent viscosity, diffusivity and solubility are characterized based on the 1D analysis used in this work, 2D experiments (e.g. cylindrical oxidation experiments of Kao [50]) can be used to quantify the stress dependent interface reaction rate. The equations described in this work can be easily extended to higher dimensions through the use of full 2 or 3D equations for the mass and momentum balance, the material law and oxidant transport. The primary difference from current 2 or 3D implementation would be the formation of an initial high density oxide at the interface, which allows the use of true “stress free” values as the base-line for oxidation parameters.

Chapter 3

Effect of Excess Density on Boron Diffusion

3.1 Introduction

Scaling metal-oxide-semiconductor field effect transistors (MOSFETS) requires the use of very thin gate oxides. For p-channel devices with p^+-polysilicon gates, a major concern is the diffusion of boron through gate oxides to the substrate causing a shift in the threshold voltage [41]. The diffusivity of boron in oxides can be modified by many factors. Increased boron diffusivity is observed when fluorine or hydrogen is introduced in the oxide [11]. In contrast, incorporation of nitrogen in SiO_2 is known [28, 45] to reduce boron diffusivity. Since it has been observed that increased oxide density strongly retards the diffusion of oxidants through SiO_2 films [4, 5], it is logical to suspect that the diffusion of other species such as boron might also be affected. In this chapter, we present the result of an experiment designed to test the effect of oxide density on boron diffusion in the oxide.

3.2 Experimental Procedure

MOS capacitors were fabricated on $4''$ $\langle 100 \rangle$ silicon wafers, with background phosphorus doping giving resistivity of 2-4 Ω-cm. A field oxide of 0.6μm was thermally grown and chemically etched to define active areas (100×100 μm^2). Thin (55–60 Å) oxides were grown in dry O_2 at 800°C, and undoped polysilicon was deposited at 625°C immediately following gate dielectric growth. Half of the wafers were then annealed for 30 min at 1100°C in N_2. We will refer to these wafers as having "relaxed" oxides, while the other half were not annealed and will be termed "unrelaxed." On each of the wafers, windows were selected to have either boron or phosphorus implanted into the polysilicon. A dose of 5×10^{15} cm^{-2} was used in both cases, with P^+ implanted at 40 keV and B^+ at 25 keV. A low temperature cap oxide of 0.5 μm was deposited at 425°C to

avoid out-diffusion of boron. Wafers were then annealed at 900°C for 12 h to allow boron penetration from the polysilicon into the substrate. After removal of the cap oxide, the polysilicon was patterned and etched, and capacitors were characterized using high frequency (100 kHz) capacitance-voltage (CV) measurements. Figure 3.1 describes the flow of the experimental procedure.

3.3 Results and Discussion

Figure 3.2 displays typical CV measurements for the relaxed and unrelaxed oxides. Also shown for reference are results with n^+ doped poly and a simulated CV curve with no boron penetration. It is evident that the sample with a relaxed oxide (i.e., with the 1100°C anneal prior to implantation) shows substantially greater voltage shifts, and thus greater boron penetration, compared to the unrelaxed sample. The fact that the phosphorus-doped capacitors show virtually identical CV curves for the relaxed and unrelaxed oxides leads us to believe that the shift observed for the p^+ doped poly can be directly attributed to changes in boron penetration.

The boron diffusivities associated with the voltage shifts in the CV curves were determined through a series of linked SUPREM IV and PISCES simulations. Effective diffusivity is defined as the boron diffusivity in SiO_2 in the SUPREM simulations for which the PISCES simulation best matched the measured CV curves. Note that the solid lines in Fig 3.2 are the results of these simulations. Figure 3.3 shows the extracted diffusivities for the relaxed (low excess density) and unrelaxed (high excess density) samples, showing about a factor of 4 difference between the two sets of samples. The error bars represent the range of values extracted for measurements on 28 capacitors of each type. Note that the larger range of values for the relaxed samples emphasizes another problem associated with boron penetration, which is that even if it is accounted for in device design, it provides an additional source of threshold voltage variation [62, 9].

Landsberger as well as Taniguchi *et al.* [4, 5, 8] conducted a series of experiments in which oxides grown at low temperatures (800 or 900°C) were found to have a substantial excess density ($\sim$4.5%), which relaxed upon annealing at higher temperatures. This relaxation was accompanied by an increase in the diffusivity and solubility of oxidizing species compared to samples which were not annealed [5]. As described in Chapter 2, we were able to model the stress relaxation process using a nonlinear dependence of viscosity on oxide density [63]. We used that analysis to match the results of single and two-step oxidation processes, as well to predict thin oxide growth kinetics. Figure 3.4 shows the predictions of that same model for the excess oxide density (averaged over the film thickness) versus annealing time during 900 and 1100°C anneals for a 54Å film grown in dry O_2. Following the initial oxide growth, the film has about 7.8% excess density. During the 30 minute 1100°C anneal, all but about 0.4% of this excess density is relaxed. In contrast, even after 12 hours the 900°C annealed oxide retains a almost 4% average excess oxide density. We believe that it is this excess density that is responsible for the reduced boron penetration compared to the 1100°C relaxed oxide.

The dependence of boron diffusivity on oxide density has an impact on the interpretation of other experimental observation. For example the strong decrease of oxide viscosity with temperature (7.4eV [60])

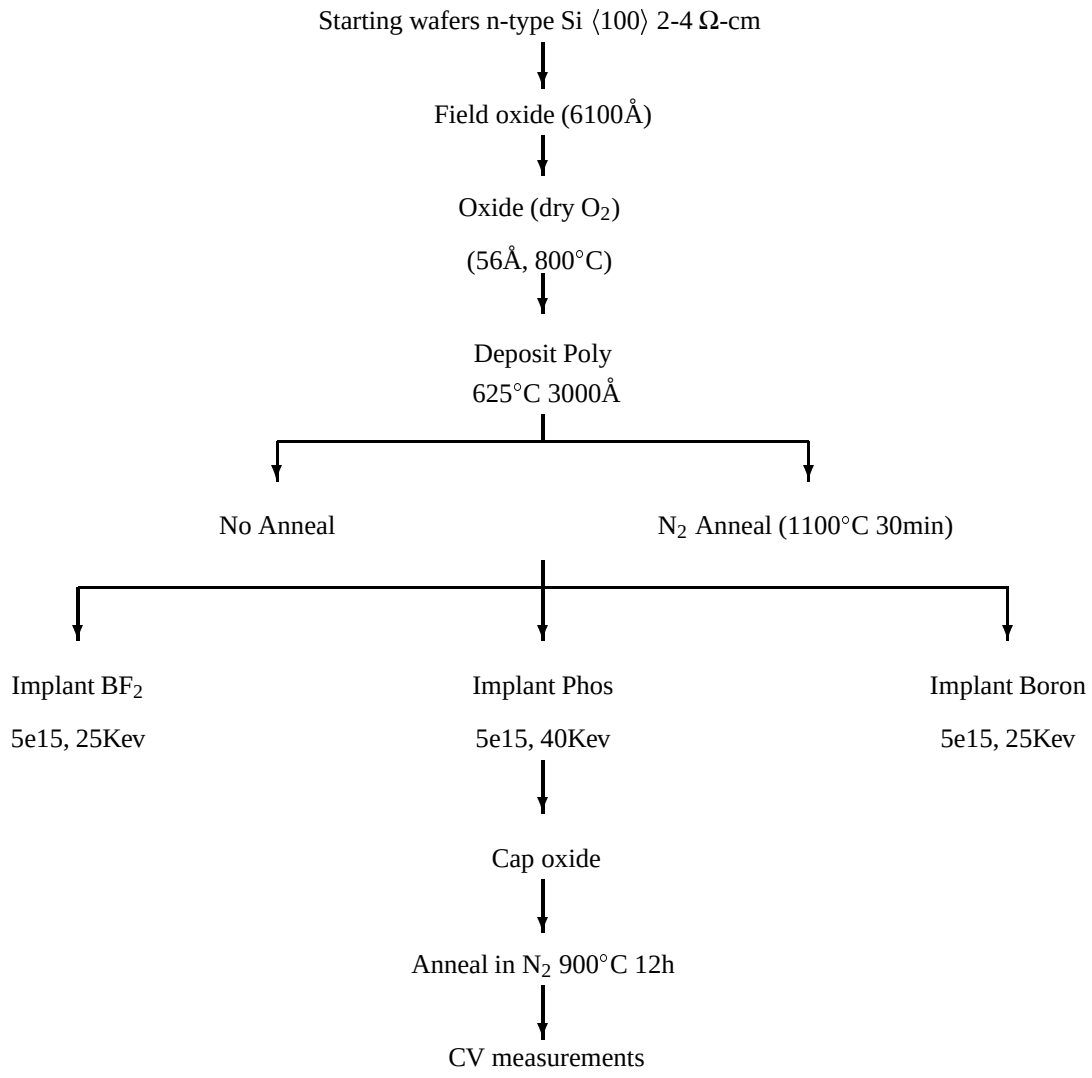

Figure 3.1: Experimental procedure for investigation of boron penetration in oxide as function of oxide excess density.

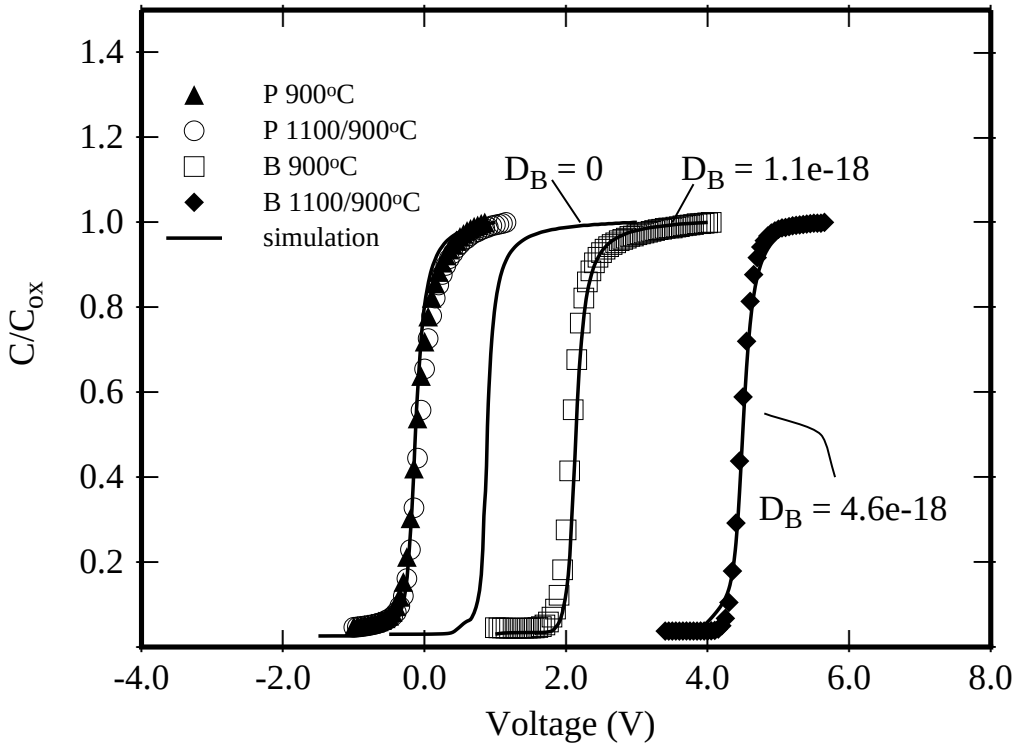

Figure 3.2: Capacitance-voltage measurements for relaxed and unrelaxed oxide annealed at 900°C. Also included are the monitor phosphorus doped capacitors for the two conditions. Lines are the simulated process/device simulation for all conditions and p^+-doped capacitor with no boron penetration.

means that a reduction in density contributes to the increase in boron diffusivity with temperature [11, 64]. In addition, Kouvatsos *et al.* [34] reported that incorporated fluorine in the oxide decreases the oxide density and refractive indexes, suggesting that enhanced oxide relaxation contributes to the increase of boron diffusion with fluorine incorporation.

Several workers [38, 11, 9, 65] have attempted to quantify the oxide thickness dependence of boron diffusion. Aoyama *et al.* [11] carried out experiments where
oxide thicknesses were varied and boron penetration was measured. They observed no oxide thickness dependence on boron diffusion. However, when fluorine was present in the system he observed a higher B diffusion for thinner oxides. They attributed this phenomena to the higher fluorine concentration for thinner oxides. Nedelec *et al.* [65] found some thickness dependence of boron diffusivity but dismissed the effect due to variations in ellipsometry measurements for thin oxides.

Fair [38] selectively combined the data from Nedelec and Aoyama and concluded that boron diffusivity is faster for thinner oxides. He described the system as follow:

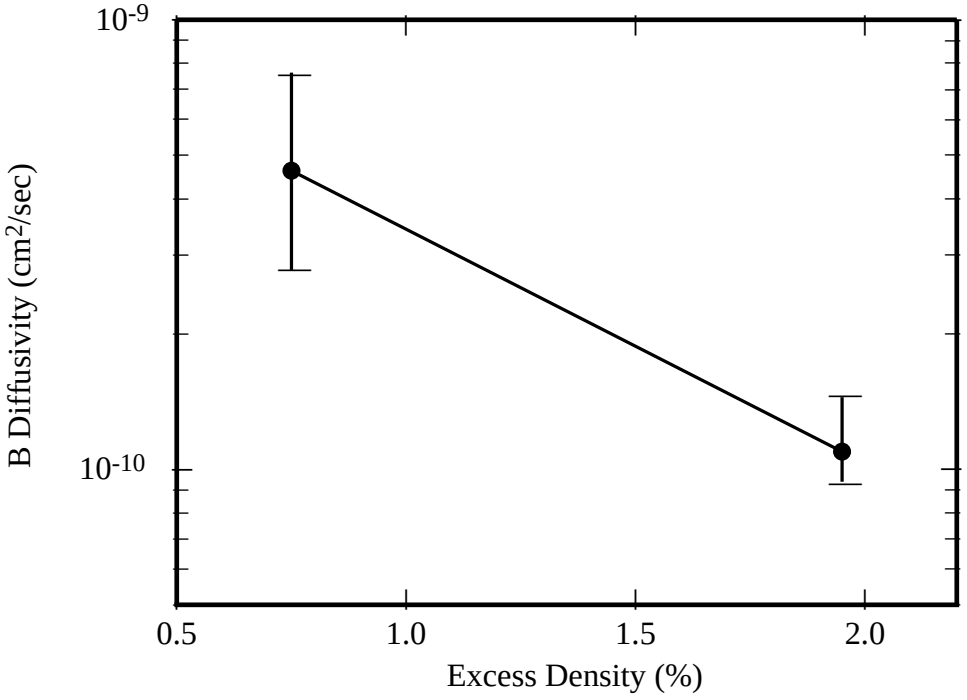

Figure 3.3: Extracted boron diffusivity in SiO_2 as a function of average excess density. Line represents an exponential change in diffusivity as function of excess density.

- Si interstitials are injected into SiO_2 during oxidation processes
- Injected Si interstitials form SiO
- As a gas SiO either reacts with O to form SiO_2 or diffuses away from the interface
- Diffusing SiO can react with the network to form defects in the oxide
- These defects (peroxy linkage defects) mediate boron diffusion in the SiO_2.

This conclusion is in contradiction with work done by Subramanian [10]. They observed a decrease in threshold voltage with decreasing channel length, a reverse-short-channel effect behavior in PMOSFETs. Based on length scales over which the V_t differences occur, they concluded that boron penetration is linked to interstitial absorption into the gate oxide (the same mechanism cited by Fair as increasing boron penetration), which reduces boron penetration at the edge of the channel compared to the middle. This leads to the observed anomalous PMOS RSCE. Figure 3.6 is a schematic for their proposed model.

Figure 3.5 shows data of Krisch *et al.* for penetration of boron as a function of thickness where BF_2 was implanted through a polysilicon gate deposited on various oxide thicknesses and annealed for 1 h 1000°C.

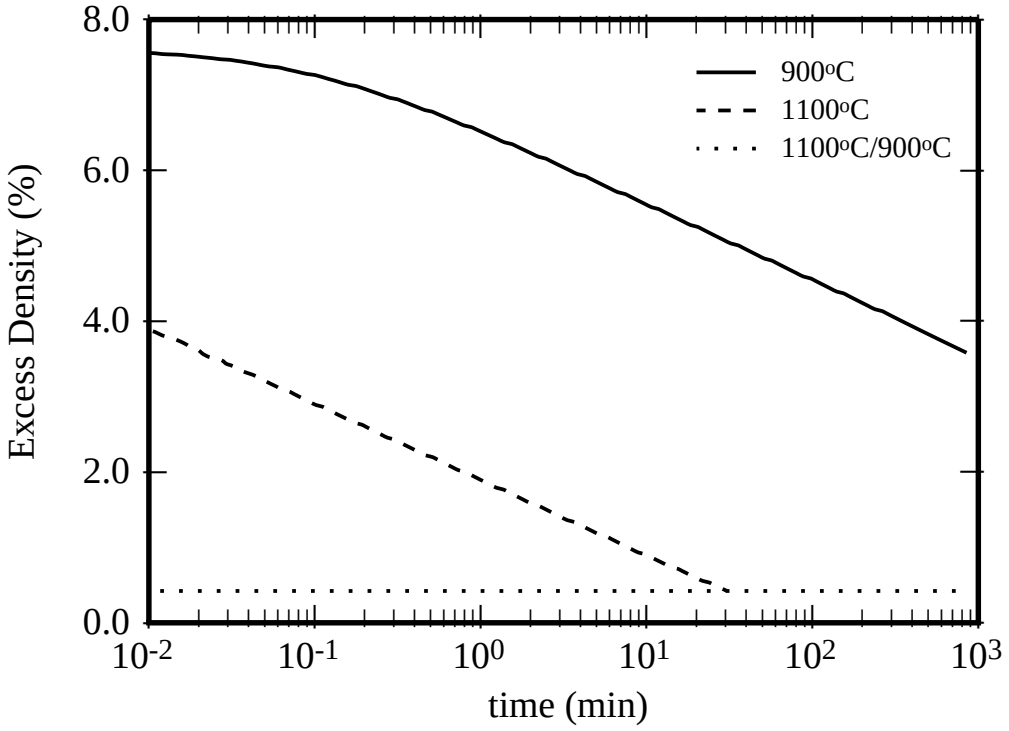

Figure 3.4: Simulation of average excess density as function of time for oxides annealed at 900 and 1100°C for 54Å oxide grown at 800°C in dry O_2. Also shown is the nearly constant density during 900°C anneal of film previously relaxed at 1100°C(dotted line).

Also shown on the same graph is a simulation assuming a thickness dependent boron diffusion of the type claimed by Fair using the same data. It is clear, from the simulation that if boron exhibited a faster diffusion for thinner oxides, the experimental data would resulted in a deviation from a straight line in the plot. Thus, again the experimental results do not support any thickness dependence for boron diffusion. Based on the full set of available data, we conclude that there is no observable thickness dependence diffusivity on boron penetration through the oxide, although there is evidence for excess silicon reducing boron diffusion.

The relaxation model presented in this work predicts that thinner oxides have larger excess density, and therefore one might conclude that this effect would result in a dependence of boron diffusivity on oxide thickness as suggested by Fair [38]. However simulations show that excess densities associated with different oxide thicknesses are relaxed to nearly the same value for annealing times larger than about one minute at 900°C (see Fig. 3.7). Since much longer annealing times are required for significant boron penetration, the changes in initial excess density associated with film thickness have negligible effect on boron diffusivity.

In modeling of the dependence of boron diffusion on oxide density, we assume that there is an activation

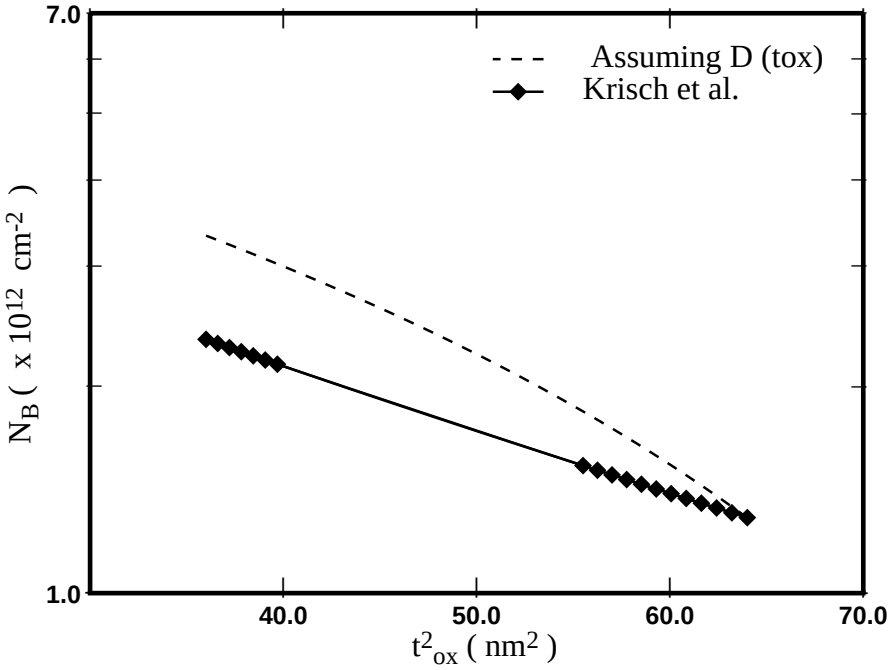

Figure 3.5: Penetrated boron as a function of oxide thickness for BF_2-implanted gates [9]. Also shown is a simulation assuming a thickness-dependent boron diffusivity for the same data.

volume associated with boron diffusion, such that the diffusivity is given by

$$D_{\mathrm{B}} = D_{\mathrm{B}}^{0} \exp(-PV_d/kT) \tag{3.1}$$

We extracted an activation volume of 27Å^3 using Eq. (1) along with the time evolution of the oxide density shown in Fig. 3.4 to match SUPREME/PISCES [66] simulation results to measured shifts in CV curves.

In conclusion, we have compared the diffusion of boron at 900°C through thin SiO_2 films grown at 800°C to equivalent films which saw an extra high temperature (1100°C) anneal. The results show that boron diffusion is increased significantly when the oxide is annealed at high temperature. The difference is attributed to excess density of oxides grown at low temperature which retarded boron diffusion in compressed oxides.

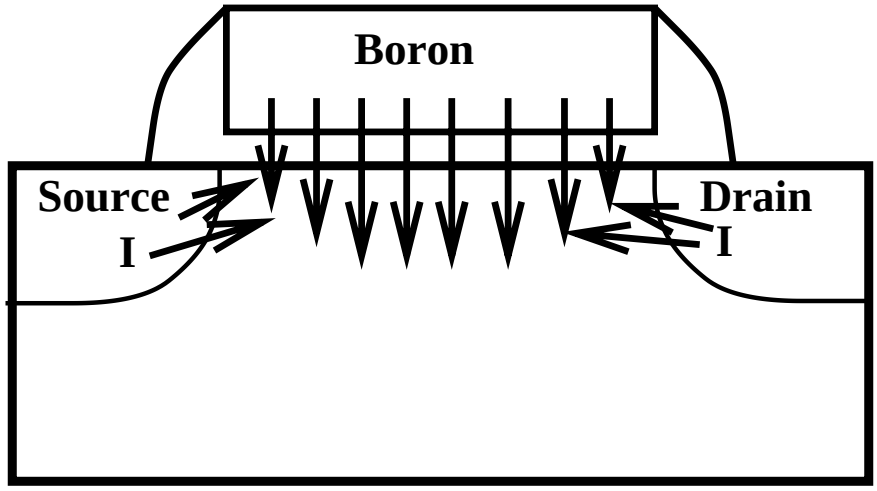

Figure 3.6: Schematic of Mechanism proposed by Subramanian [10] for PMOS RSCE, where Si interstitials are absorbed into the gate oxide at the edges, blocking boron penetration.

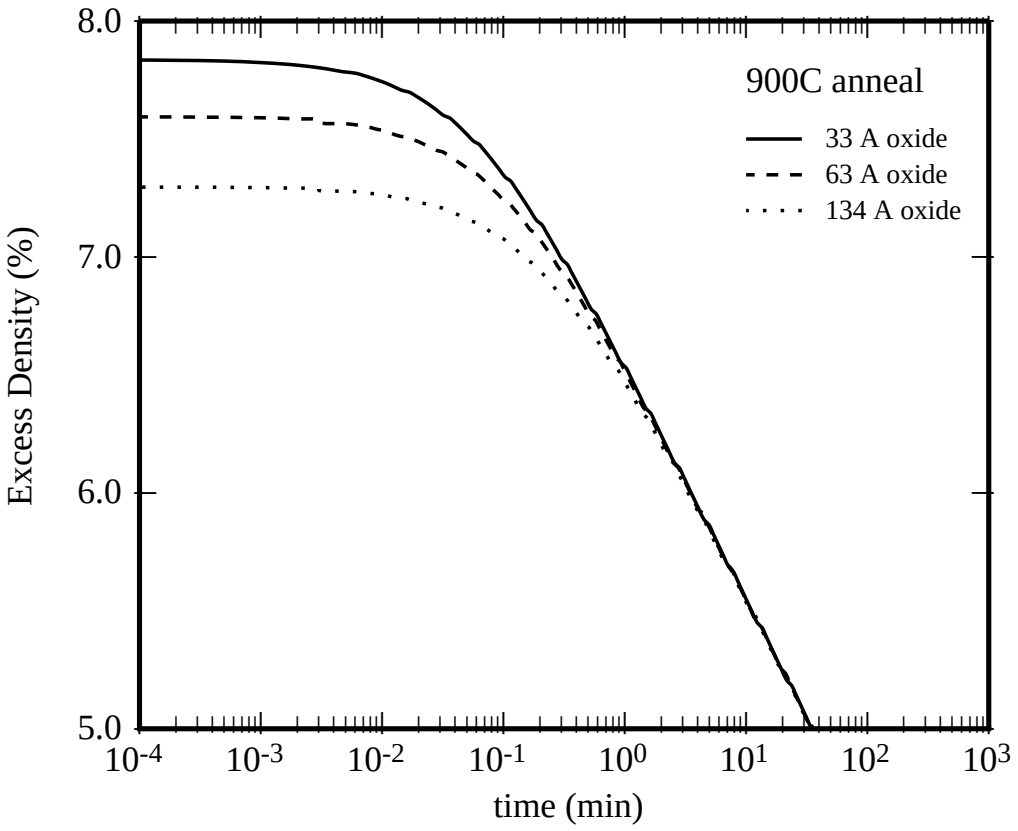

Figure 3.7: Simulation of excess density as function of time during annealing at 900°C for various oxide thicknesses originally grown at 800°C.

Chapter 4

Nitrogen Incorporation

4.1 Introduction

As gate oxide dimensions in metal-oxide-silicon field effect transistors (MOSFETs) continue to shrink, the issue of boron diffusion from the polysilicon gate to the Si channel in pMOSFETs is becoming increasingly important. The boron in the polysilicon can be driven into the gate oxide as well as the substrate if thermal cycles exists after source/drain implantation. Although low thermal budget processing is always desirable, its complete elimination is hardly possible. These thermal cycles include, gate oxidation, dopant activation, spacer formation and interlevel-dielectric densification and reflow, etc. [67]. The signature of boron penetration in p-MOSFETS is often recognized by threshold voltage instabilities [21] and subthreshold swing degradation [41].

There are many approaches to reduce boron penetration. The most obvious is to lower the thermal budget subsequent to oxidation. Alternatively, manipulating the crystalline structure of polysilicon gate can be somewhat effective in reducing boron penetration [68, 69]. However, one of the most effective approaches, and also the one of the least understood, is the introduction of nitrogen into gate oxide. There are many ways of introducing of nitrogen plasma NH_3 nitridation [28], thermal NH_3 nitridation [45], oxidation in NO [70] and N_2O [71] ambients. Although B diffusion is expected to depend locally on the oxide structure and composition, modeling to date has been generally limited to determining an effective average diffusivity as a function of processing conditions [45, 38]. To generate a predictive model, it is important to consider the underlying oxide composition and structure that results in the observed diffusivity. In order to help address these issues, we have conducted a series of experiments in which both boron diffusivity as well as the composition of the oxide were studied.

4.2 Experimental Procedure

MOS capacitors were fabricated on $4^{''}$ $\langle 100 \rangle$ silicon wafers, with background phosphorus doping of 2–4 Ω-cm. A field oxide of 0.6μm was grown and etched to define active areas (100×100 μm^2). Gate dielectrics were grown in pure O_2 at 870°C, pure N_2O at 910°C or an N_2O/O_2 at 870°C mixture. Undoped polysilicon was deposited at 625°C immediately following gate dielectric growth. The polysilicon was implanted to a dose of 5×10^{15} cm^{-2}, using P^+ at 40 keV and BF_2^+ or B^+ at 25 keV. A low temperature cap oxide of 0.5 μm was deposited at 425°C to avoid out diffusion of boron. Wafers were annealed at 900-1050°C for various times to insure boron penetration. After removal of the cap oxide, the polysilicon was patterned and etched. Aluminum deposition followed by sintering was performed on some samples and capacitor-voltage measurements showed no difference between capacitors with and those without aluminum electrodes. Figure 4.1 describes the flow of the experimental procedure.

Capacitors were characterized using high frequency (100 KHz) capacitance-voltage (CV) measurements. In addition, SIMS measurements were carried out[1] to quantify the amount of nitrogen and boron incorporation in the gate oxides, as well as in the polysilicon and substrate.

4.3 Secondary Ion Mass Spectroscopy Measurements

Secondary Ion Mass Spectroscopy (SIMS) was used for profiling of nitrogen, fluorine and boron in this work. The SIMS analysis was done at Evans East. The samples were sputtered with either oxygen or cesium ion bombardment. More detailed description of the method is included in Appendix B.

4.3.1 Boron Profiling in Oxide

To gain insight into the process of boron penetration in gate dielectric we attempted to profile boron in oxide using SIMS measurements. As described previously, oxide and oxynitride dielectrics deposited. The implanted into out in N_2 at measurements, analysis of the gate the deposited Hydroxide selectivity to oxide [72]. about 80°C. All cleaved wafers were 7:1 prior to the etching process to ensure clean surface. Due to the selectivity of TMAH we believe that amount of dielectric has been etched. Furthermore, ellipsometry measurements of thin gate dielectrics before and after dip in TMAH for more than a minute showed very similarly gate dielectric thickness.

As described in Appendix B, $O_2{}^+$ bombardment was used to sputter the has greater sensitivity for samples [73]. show the boron as well as the in gate dielectric grown in profiles measured on the samples high concentration at the surface, the dielectric/silicon interface.

Close examination of Figure 4.2 and 4.3 show that slope of boron profile is very similar to that of the oxygen signal for depth greater than 40Å. The slope of the oxygen signal is an artifact of knock-on and mixing effects during sputtering which result in loss of depth resolution. In reality one might expect the

[1] Performed by Evans East, Plainsboro, NJ.

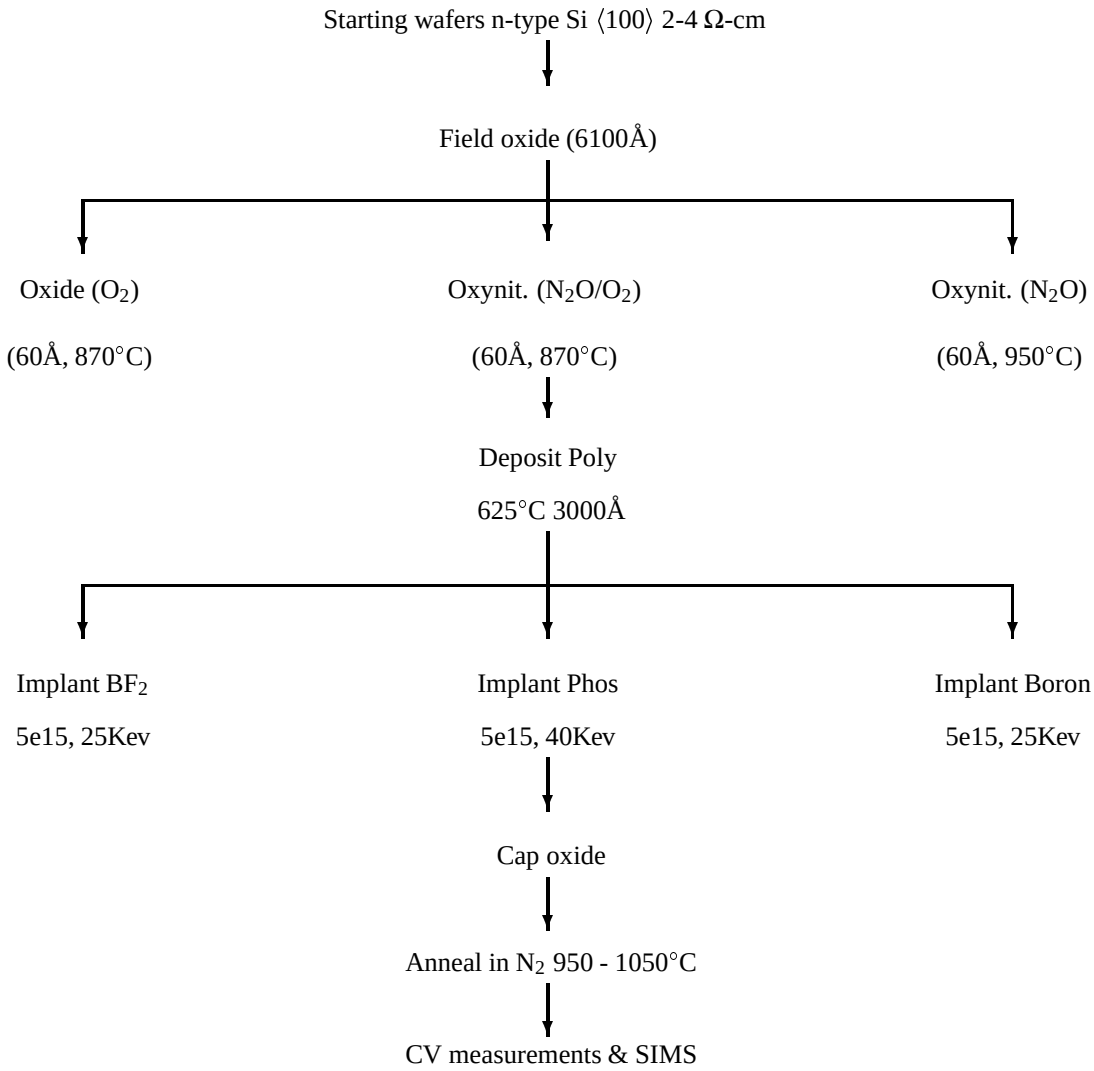

Figure 4.1: Experimental procedure for investigation of boron penetration in oxide as function of incorporated nitrogen and fluorine

interface to be quiet abrupt. The similarity of the boron and oxygen profiles leads us to believe that the boron profiles in these regions are not accurate and are limited by the SIMS depth resolution. Thus, no firm conclusion could be made from our SIMS data regarding the profile of boron in the dielectrics.

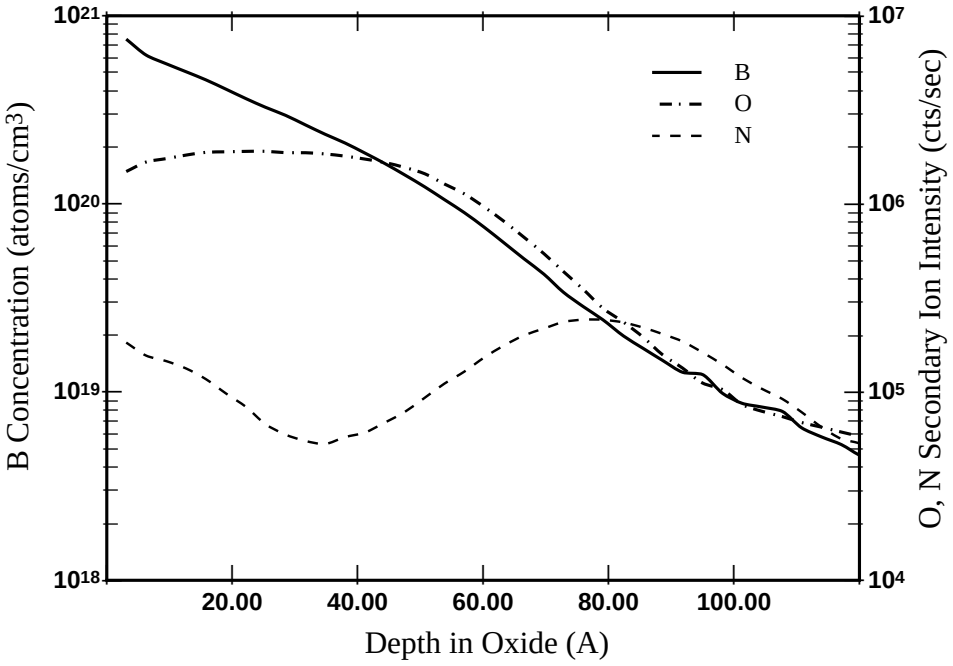

Figure 4.2: SIMS profile of boron, nitrogen and oxygen in a 60Å dielectric grown in N_2O ambient which was annealed at 950°C.

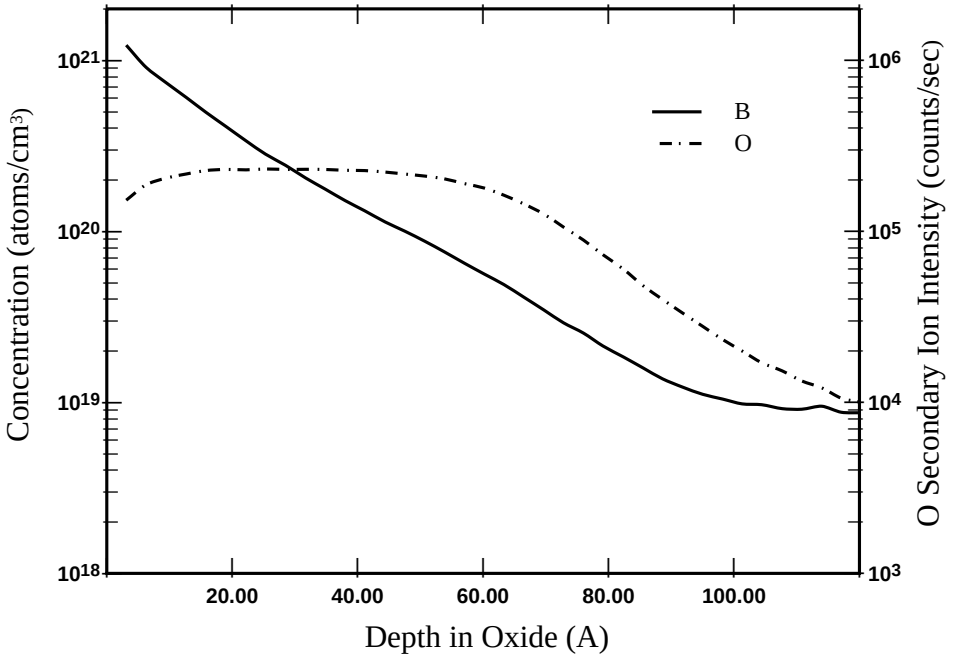

Figure 4.3: SIMS profile of boron and oxygen in a 60Å oxide grown in dry O_2, which was annealed at 950°C.

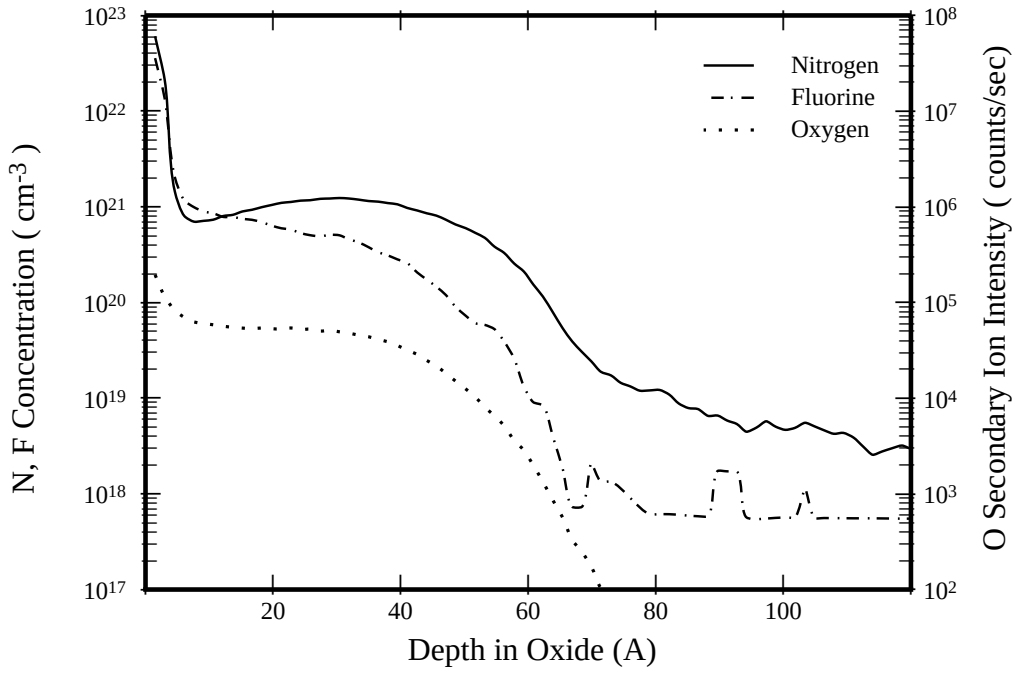

Figure 4.4: SIMS profiles of nitrogen, fluorine and oxygen in oxynitride annealed for 120 minutes in N_2 at 950°C.

4.3.2 Nitrogen Profiling in Oxide

The gate stack structures of poly/oxide/Si were fabricated to study boron penetration through thin gate dielectrics. Following implantation of B or BF_2 in the polysilicon, the structure was annealed in inert ambient to ensure boron penetration. For SIMS analysis, polysilicon was removed using TMAH as described in previous section. SIMS analysis were carried out to determine the profile of nitrogen and fluorine in the gate dielectric using Cs^+ primary ion bombardment with positive secondary ion detection.

Figure 4.4 shows an example SIMS profile for an oxide grown in 100% N_2O with a $5 \times 10^{15}cm^{-2}$ BF_2 implant in the polysilicon. It can be noted that incorporated nitrogen is relatively uniform through out the film but peaks somewhat closer to the Si/SiO_2 interface. Also shown as reference is the intensity of the oxygen signal.

To investigate the effect of nitrogen incorporation on boron diffusivity, we grew gate dielectrics with different amounts of incorporated nitrogen. Figure 4.5 shows the comparison of two gate dielectrics grown in 100% N_2O and 20/80% N_2O/O_2. The corresponding average nitrogen content for the samples are 1.4% and 0.2%, respectively. Finally to better understand the time evolution of incorporated nitrogen we carried out experiments, where gate dielectric grown at 100% N_2O

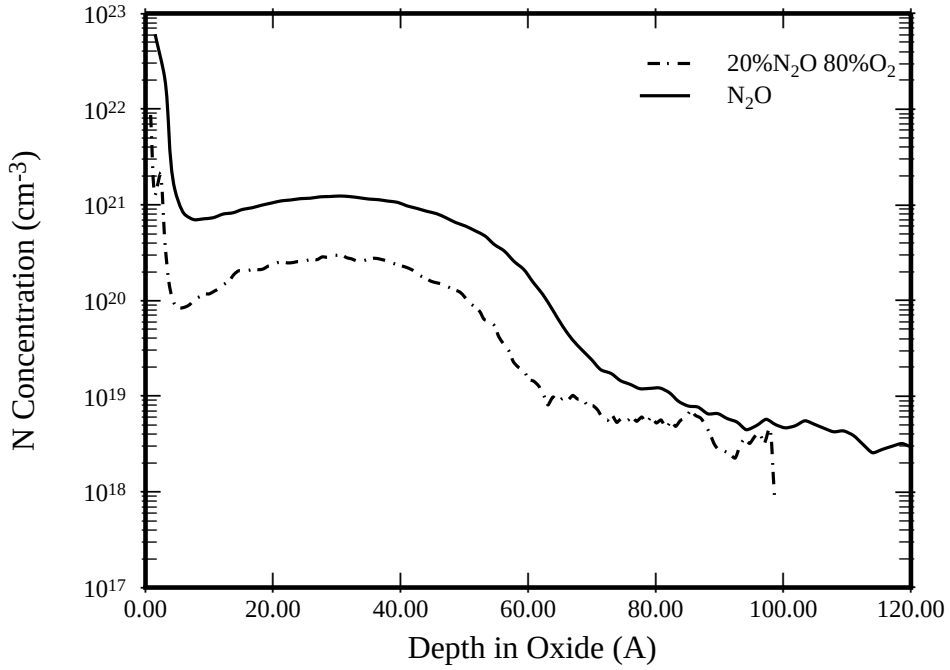

Figure 4.5: Incorporated nitrogen concentration for dielectrics grown in 100% N_2O and 20/80% N_2O/O_2.

were annealed at 950°C for 5 and 10 hours. Results are shown in figure 4.6. It can be noted that the nitrogen profiles in the dielectric remain unchanged as function of annealing time, in contrast to reports from Ellis *et al.*. for 1000°C annealing (5h) which showed substantial nitrogen loss [12].

4.3.3 Fluorine Profiling in Oxide

To better understand the effect of fluorine we conducted a series SIMS measurements. Figure 4.7 shows a comparison of fluorine profiles for an oxide grown in 100% O_2 versus a dielectric grown in 100% N_2O. While the nitrogen concentration is relatively uniform throughout the film peaking somewhat closer to the Si/SiO_2 interface, the fluorine shows an approximately linear behavior. This suggests that fluorine diffuses through the thin dielectric into the substrate. This linear behavior is also seen for dielectrics grown in a pure O_2 ambient. It can be observed that oxide films in an N_2O ambient appear to incorporate a slightly lower level of fluorine. This behavior may be attributable to a difference in segregation of fluorine to oxides versus oxynitrides.

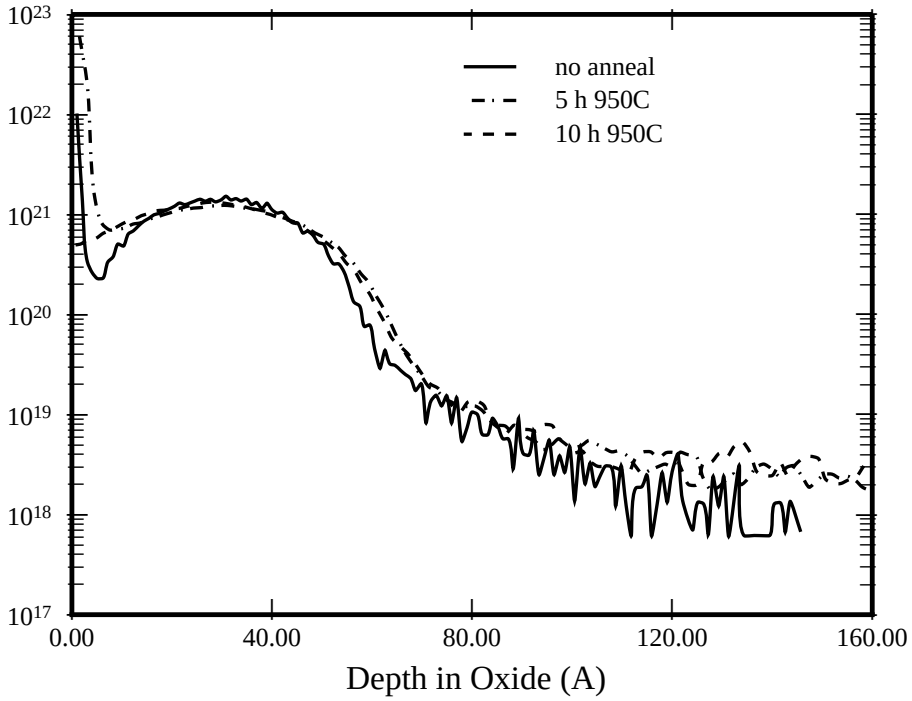

Figure 4.6: SIMS profiles of N in oxynitrides grown in pure N_2O and annealed for 5 and 10 hours at 950°C.

4.4 Capacitor Voltage Measurements

In this work, Capacitor voltage measurements were extensively used to characterize boron diffusion in gate dielectrics. Appendix B describes the details of the CV measurements used in this work.

4.4.1 Extracted Diffusivity

The diffusivity parameters in this work were extracted by comparing the result of linked SUPREM IV and PISCES simulations to the experimental CV curves. Effective diffusivity is defined as the B diffusivity in oxide which best predicts the shift of the CV curves. Although we believe boron diffusivity depends on local impurity incorporation (e.g. nitrogen and fluorine) we extracted this parameter to better compare our results with the work of other researchers.

Figure 4.8 shows the extracted effective boron diffusivity versus temperature. Also shown in Figure 4.8 are the extracted diffusivity values reported by Aoyama *et al.* [11]. Although B diffusivity in both oxide and oxynitride agree very well with the reported values of Aoyama *et al.* [11], the BF_2 samples show a different activation energy (2.07 compared to 3.65 for oxide and 1.3 compared to 3.75 for oxynitride). This may be attributable to the redistribution of fluorine in the system over time (see discussion of fluorine redistribution in the next chapter).

Diffusivity of boron depends strongly on the composition of gate dielectric. When fluorine is present in the oxide, the diffusivity of boron is enhanced (only 35 min. were required for substantial boron penetration at

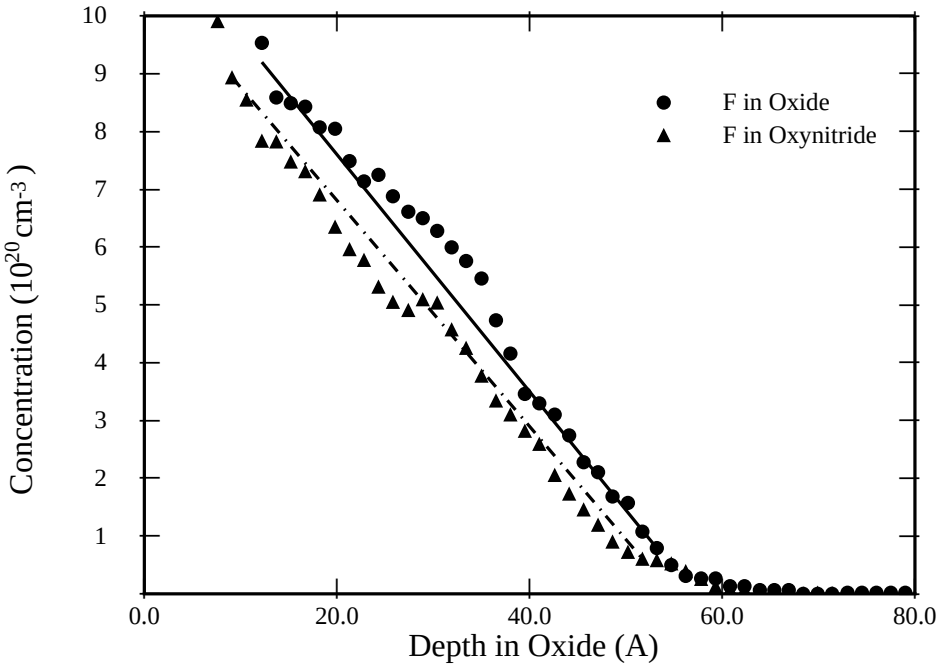

Figure 4.7: Comparison of incorporated F in gate dielectrics grown in either O_2 or N_2O and annealed at 950°C in N_2 for 35 and 125 minutes, respectively.

950°C). However, when a sufficient amount of nitrogen is incorporated in the gate dielectric, boron diffusivity is reduced (the samples were annealed for 10 h to insure significant boron penetration). Table 4.1 summarizes the experimental conditions, as well as the effective boron diffusivity for each sample.

It has been shown that species like fluorine and chlorine, which are used during oxidation of silicon, enhance the oxidation rates [33]. These species can effectively substitute for oxygen and act as network terminators, thus modifying the structure of the oxide and allowing the oxidizing species to diffuse faster. The resulting increase in the flexibility of the oxide network in presence of fluorine would also be expected to increase the diffusivity of boron. Nitrogen, on the other hand is known to both strengthen the oxide network and reduce the diffusivity of boron in the gate dielectric [11, 9, 65].

To investigate the effect of nitrogen incorporation on boron diffusivity, we grew gate dielectrics with different amounts of incorporated nitrogen. Figure 4.5 shows the comparison of two gate dielectrics grown in 100% N_2O and 20/80% N_2O/O_2. The corresponding average nitrogen content for the samples are 1.4% and 0.2% respectively. Extraction of effective boron diffusivity for these samples showed that a certain amount of nitrogen incorporation (on the order of 1% or more) is required to significantly reduce boron penetration

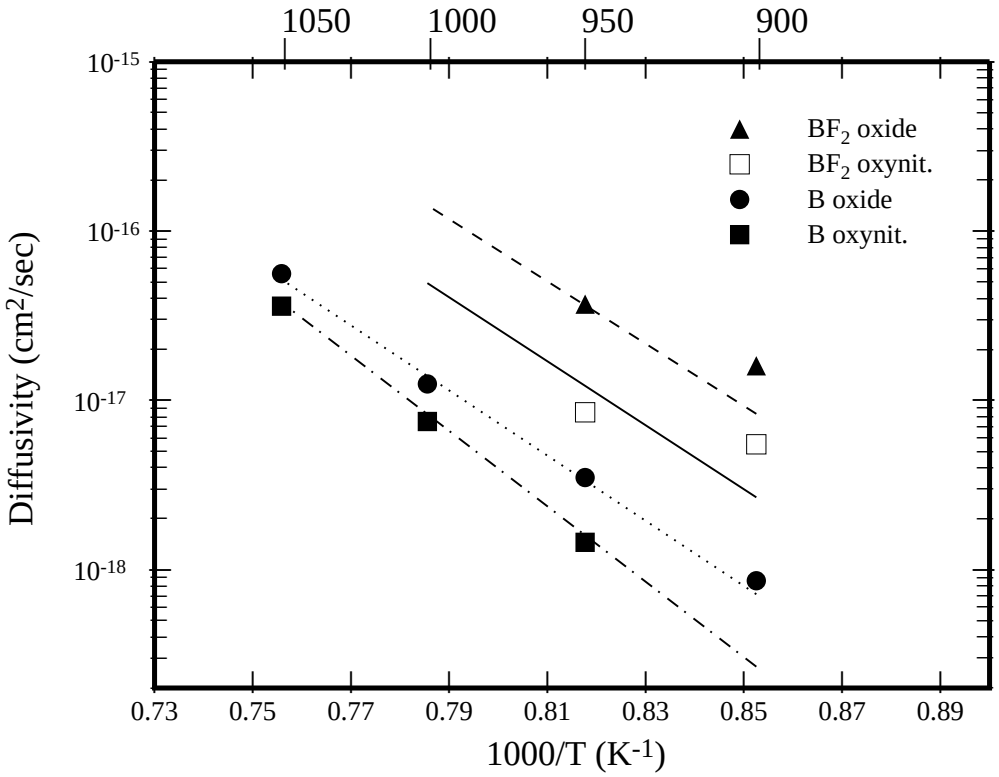

Figure 4.8: Effective boron diffusivity for gate dielectrics grown in dry O_2 at 870°C and N_2O at 910°C as function of temperature. Values are extracted from shift of CV curves. Also shown for comparison (lines) are data from Aoyama *et al.* [11] for corresponding conditions.

compared to that of a oxide grown in pure O_2. The extracted boron diffusivity as a function of nitrogen content is shown in Figure 4.9. Close inspection of Figure 4.9 reveals that the effect of nitrogen is more pronounced when fluorine is present in the system. In the case of BF_2 implants the boron diffusivity in oxynitride is reduced by a factor of 4.3 compare to that of oxide grown in pure O_2, while when boron is implanted in polysilicon, this factor is only 2.4 times. Another notable feature that can be seen in Figure 4.8, is that the effectiveness of nitrogen to block boron diffusion in SiO_2 drops substantially at higher temperatures. This presents a dilemma for device fabrication, since relatively high temperature rapid thermal anneals (RTA) are desirable to limit transient enhanced diffusion of boron in the substrate.

4.5 Lattice Monte Carlo Simulations

Lattice Monte Carlo (LMC) simulations replicate the details of the critical atomistic processes, and thus one can use LMC simulations to explore the macroscopic implications of the processes occurring at the atomistic level. In particular, LMC calculations can be used to provide a check on some of the modeling assumptions

Implant	**% N**	x_{ox} **(Å)**	**Time (min)**	**Temp**°C	D_B **(10^{-18}cm^2/s)**
BF_2	0	55	35	950	37
BF_2	0.2	60	80	950	3.7
BF_2	1.4	55	125	950	8.5
BF_2	0	75	60	900	16
BF_2	1.4	74	200	900	5.5
B	0	60	315	950	3.5
B	0.2	60	360	950	3.1
B	1.4	60	615	950	1.45
B	0	55	40	1000	12.5
B	1.4	50	60	1000	7.5
B	0	77	30	1050	56
B	1.4	74	30	1050	36

Table 4.1: Extracted boron diffusivity values for different experimental conditions

and parameter values used in continuum simulations. In the case of boron diffusion in gate dielectrics, we believe that N and F affect B diffusion in oxides by locally stiffening or relaxing, respectively, the oxide network and thus retarding or enhancing B diffusion.

It has been shown [74, 12] that the formation of B-N bonds is energetically unfavorable. It has also been suggested [74] that boron substitution into a Si-N site would require more energy than substituting into a nitrogen free site. Based upon these observations, Ellis *et al.* [12] used a lattice Monte Carlo model in which diffusion of boron atoms was blocked by the presence of nitrogen in the system. In this model the presence of Si-N bonds in the lattice resulted in prevention of boron substitution. They found their results matched their observation of boron diffusion at relatively high temperature (1050°C).

To model diffusion of boron in oxynitride as function of incorporated nitrogen and fluorine we also conducted Lattice Monte Carlo simulations adapting the software from Bunea and Dunham [75]. The silicon atoms were modeled in a diamond structure giving a quartz structure. Although this is not a precise reconstruction of the amorphous oxide network, it can be used as a qualitative tool to relate boron diffusion to amount of impurity incorporation in oxide. The simulation lattice was constructed from a three dimensional ($10\times50\times50$) array of cubic cells each containing 8 atoms. Periodic boundary conditions were used at the edges. The appropriate amount nitrogen or fluorine was distributed randomly throughout the lattice. Finally boron atoms were introduced into the system.

In this system, boron diffusivity is reduced in presence of nitrogen atom by

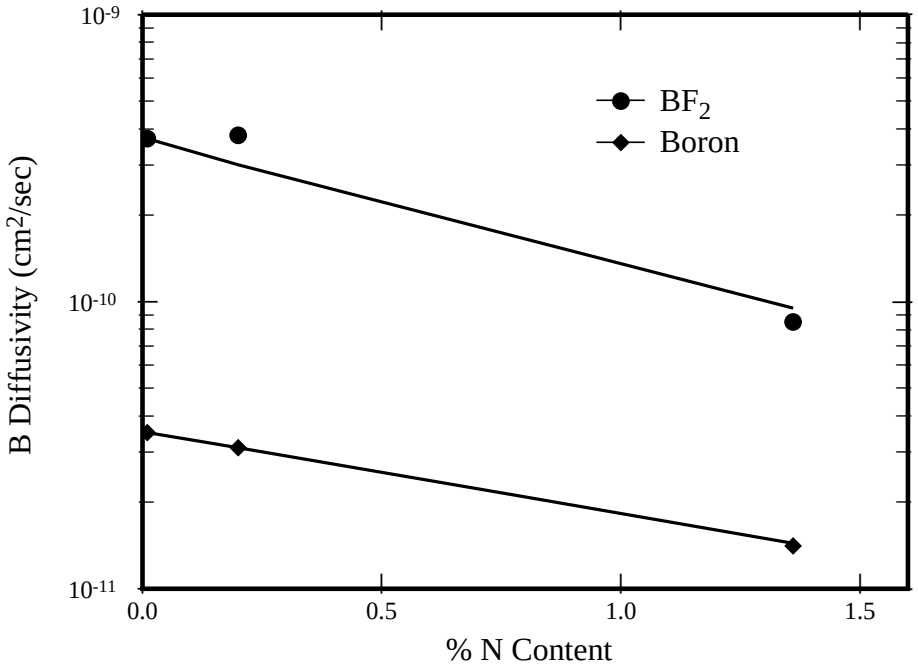

Figure 4.9: Comparison of boron diffusivity in gate dielectric as a function of average nitrogen content. Samples were annealed at 950°C.

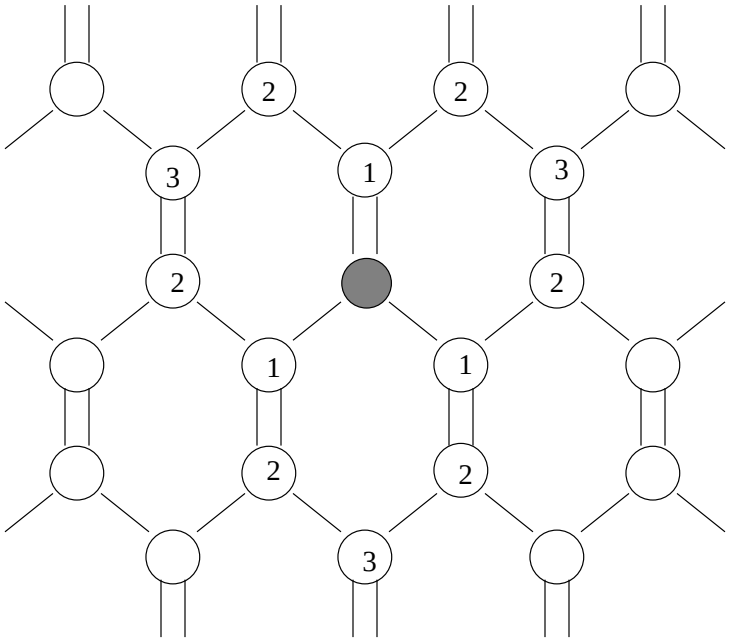

Figure 4.10: Schematic of the lattice structure used in Lattice Monte Carlo simulation of oxide. Nitrogen atoms are distributed randomly throughout the lattice. Boron diffusion is reduced locally increasing the migration energy.

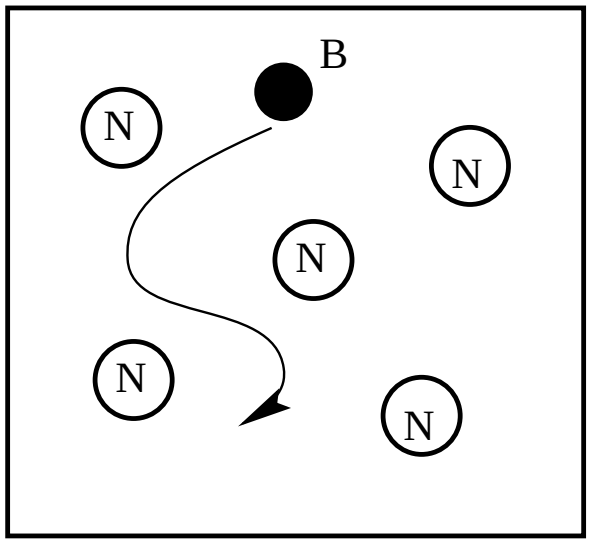

Figure 4.11: Schematic of boron diffusion through silicon dioxide structure where nitrogen slows diffusion in nearby sites.

reducing the hopping frequency whenever a boron is near a nitrogen atom. This reduction is extended up to sixth nearest neighbor (6NN) blocking with migration energy varying inversely with distance from nitrogen atoms. ($\Delta G_m \sim 1/R$ see Figures 4.10 and 4.11).

The results are shown in Figure 4.12 comparing the effect of nitrogen on boron diffusion using Ellis's blocking model as well as the local stiffening model developed in this work. Ellis *et al.* were able to account for their data by including effectively only nearest neighbor (1NN) interactions. Inspection of boron diffusion in the presence of nitrogen shows that the effect of nitrogen is much more pronounced at lower temperatures. Ellis *et al.* were able to explain data at higher temperatures (specifically 1050°C), but at lower temperatures local blocking is not sufficient to account for the observed behavior and more long range effects must be included. We found that considering up to 6NN interaction gave results consistent with experimental observations.

Lattice Monte Carlo simulation were also used to study the effect of fluorine incorporation on boron diffusion in oxide. In the presense of fluorine, boron diffusion was increased, with the increase extending again up to the sixth nearest neighbor distance. Figure 4.13 shows the result of LMC simulations for boron diffusion in presence of fluorine.

Applying the above model, we found that B diffusion can be expected to vary with N and F concentrations as

$$D_{\mathrm{B}} = D_{\mathrm{B}}^{0} \exp(-C_{\mathrm{N}}/C_{\mathrm{N}}^{\mathrm{ref}}) \tag{4.1}$$

and

$$D_{\mathrm{B}} = D_{\mathrm{B}}^{0} \left[1 + (C_{\mathrm{F}}/C_{\mathrm{F}}^{\mathrm{ref}})^{1.6}\right], \tag{4.2}$$

with $C_{\mathrm{N}}^{\mathrm{ref}}$ and $C_{\mathrm{F}}^{\mathrm{ref}}$ decreasing with both the magnitude and range of the local retardation factors.

Due to the high solubility and low diffusivity of boron in the oxide, one can model the system in terms of a continuity equation:

$$\frac{\partial C_{\mathrm{B}}}{\partial t} = \frac{\partial}{\partial x} D_{\mathrm{B}} \frac{\partial C_{\mathrm{B}}}{\partial x}, \tag{4.3}$$

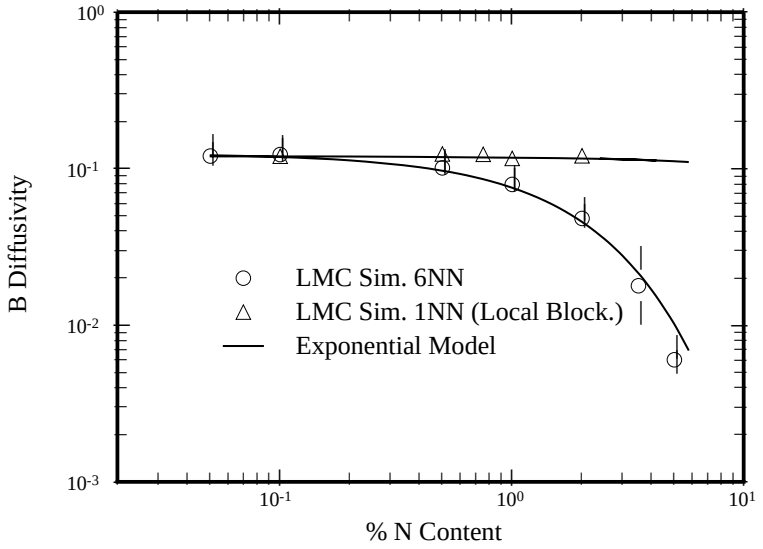

Figure 4.12: Lattice Monte Carlo simulation for boron diffusion in oxynitride. The plot shows comparison of first nearest neighbor blocking (as in Ellis *et al.* [12]) and sixth nearest neighbor blocking.

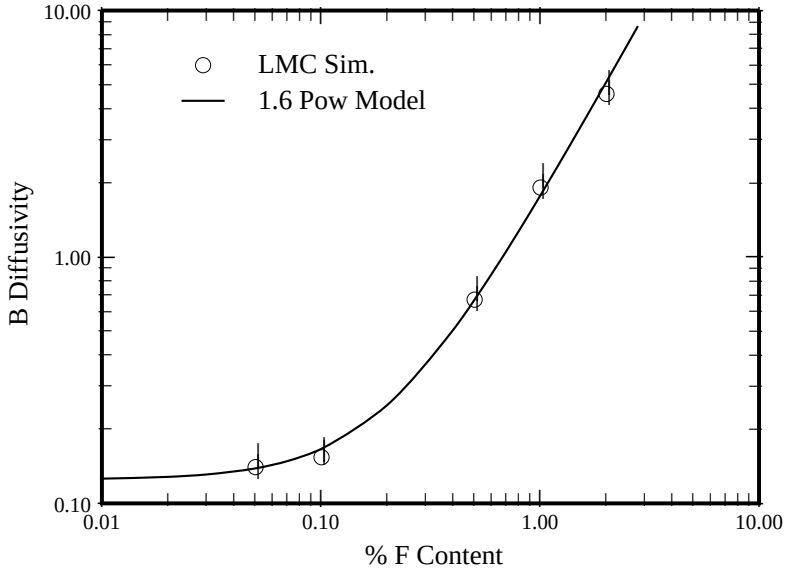

Figure 4.13: Lattice Monte Carlo simulation of boron diffusion in presence of fluorine and comparison to analytic function.

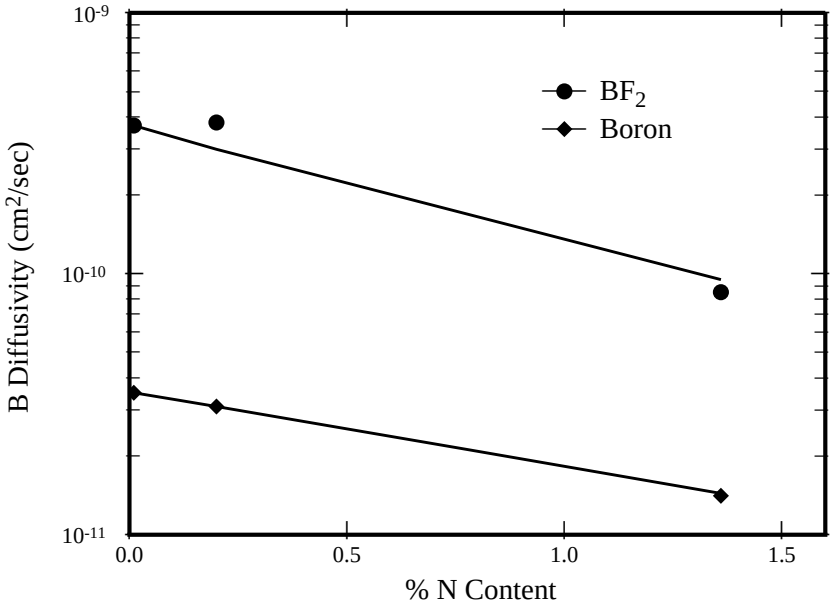

Figure 4.14: Comparison of boron diffusivity in gate dielectric as a function of average nitrogen content. Samples were annealed at 950°C. Lines represent changes in diffusivity due to nitrogen and fluorine concentration as in equations 4.1 and 4.2.

where C_B is boron concentration and D_B is boron diffusivity in the oxide. Boron diffusivity is then modeled as a function of local composition and structure from equations 4.1 and 4.2.

The above model was implemented in the PDE solver DOPDEES [76] and matched to data as shown in Figure 4.14. Although one might suspect an interaction between nitrogen and fluorine in the system we were able to fit the data assuming that the effects multiply (energies add) which suggests that these interactions are negligible at 950°C temperature for the nitrogen and fluorine levels used in this work.

4.6 Conclusions

To investigate the role of fluorine and nitrogen, we conducted a series of experiments using both B and BF_2 implanted into polysilicon and diffused through dielectrics grown in pure O_2, pure N_2O and a mixed N_2O/O_2 ambient. The extracted boron diffusivities were measured via CV measurements. SIMS analysis were performed to obtain the profiles of fluorine and nitrogen in the dielectric for the same samples. The results show that a significant amount of incorporated nitrogen (on the order of 1% or more) is required to significantly reduce boron diffusion in the gate dielectric.

We have also investigated the role of fluorine redistribution in this system. Although nitrogen incorpora-

tion is fairly uniform in the gate dielectric, the profile of fluorine shows a linear behavior. This suggests that fluorine diffuses readily through the gate oxide. Its distribution in the oxide thus depends on the segregation from the poly to the oxide and its concentration in the poly.

In order to understand how impurity incorporation would change the B diffusivity, we used LMC simulations of B diffusion through an oxide network with randomly located N and/or F atoms which locally reduced or enhanced the B hopping rates. We used the result of LMC calculation in a continuum model and were able to predict boron diffusion as a function of local impurity incorporation.

Chapter 5

Fluorine Incorporation

5.1 Introduction

It has been shown that species like fluorine and chlorine, which are used during oxidation of silicon, enhance the oxidation rates [33]. These species can effectively substitute for oxygen and act as network terminators, thus modifying the structure of the oxide and allowing the oxidizing species to diffuse faster. The resulting increase in the flexibility of the oxide network in presence of fluorine would also be expected to increase the diffusivity of boron.

The source of incorporated fluorine is actually in the top polysilicon layer. However, role of fluorine in polysilicon or silicon systems has been less characterized. This chapter examines the kinetics of redistribution of fluorine in poly/SiO_2Si structure to better understand how boron diffusion is effected in presence of fluorine.

5.2 Experiments

To investigate the redistribution of fluorine in the poly/SiO_2/Si system, we carried out experiments in which BF_2 implanted into the polysilicon was annealed for 20 and 80 minutes at 950°C. Resulting SIMS profiles for both fluorine and boron are shown in Figure 5.1.

Inspection of SIMS profile shows that boron diffuses very rapidly in polysilicon, resulting in a nearly flat profile in this region. It may also be noted that boron diffused through the gate oxide and penetrated into silicon substrate for both anneal times. Fluorine species however, appear to have a low solid solubility along with fast diffusion in the polysilicon and silicon. There is also very strong segregation to the oxide. The other dominate feature in the SIMS data is the aggregated fluorine near the original implant peak.

As long as aggregated fluorine remains near the initial implant peak, its concentration in the poly remains approximately constant (corresponding to a solid solubility concentration), which in turn keeps a steady profile of fluorine in the oxide. For longer times, it is expected that all the fluorine will eventually be lost

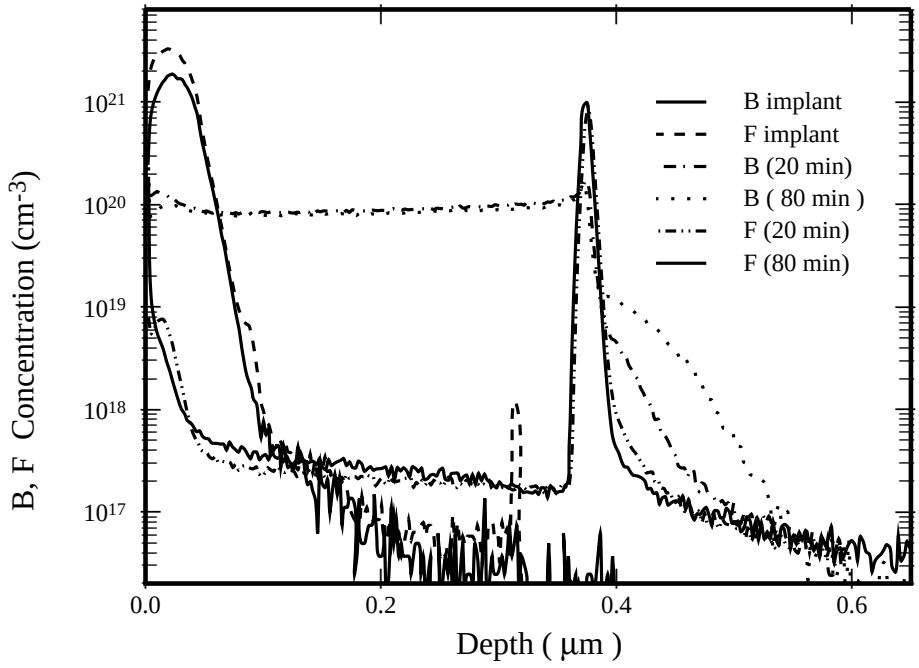

Figure 5.1: SIMS profiles of boron and fluorine distribution in poly/SiO_2/Si system following 20 and 80 minutes anneals at 950°C. As-implanted profiles are also shown.

to the substrate, resulting in a concentration drop in both the oxide and the polysilicon. This behavior may explain the observation by Aoyama *et al.* [11] that boron diffusion appears slower for thicker films. Much longer annealing times are required to observe boron penetration in thicker films, and longer annealing times result in a loss of fluorine to the substrate and a subsequent drop in fluorine concentration in the oxide, reducing the overall boron diffusivity. In addition, the reported linear dependence of boron diffusivity on the implanted fluorine dose in the polysilicon reported by Aoyama *et al.* [11] may be attributable to the time required for fluorine to escape to the substrate and/or oxide layers. At higher doses, fluorine is present for longer time resulting in larger overall boron diffusivity compared to lower doses.

5.3 Modeling

To account for the fluorine behavior we modeled F redistribution in poly/SiO_2/Si by assuming a fast diffusion of F in both polysilicon and silicon. We implemented a one moment clustering model [76] for fluorine diffusion in polysilicon.

$$F + F \leftrightarrow C \qquad \text{nucleation} \tag{5.1}$$

$$F + C \leftrightarrow C \qquad \text{growth} \tag{5.2}$$

were F is fluorine and C is a cluster of fluorine atoms. Writing the transport equation for fluorine

$$\frac{\partial C_{\mathrm{F}}}{\partial t} = \frac{\partial}{\partial x} D_{\mathrm{F}} \frac{\partial C_{\mathrm{F}}}{\partial x} - R_1 - R_2 \tag{5.3}$$

where C_{F} is concentration and D_{F} is diffusivity of fluorine. The equation describing the evolution of the fluorine clusters is;

$$\frac{\partial C_{\mathrm{clus}}}{\partial t} = R_1 + R_2 \tag{5.4}$$

where

$$R_1 = \quad 2k(C_{\mathrm{F}}^2 - C_{\mathrm{ss}}^2) \quad \text{if } C_{\mathrm{F}} > C_{\mathrm{ss}} \tag{5.5}$$

$$0 \qquad \text{if } C_{\mathrm{F}} < C_{\mathrm{ss}} \tag{5.6}$$

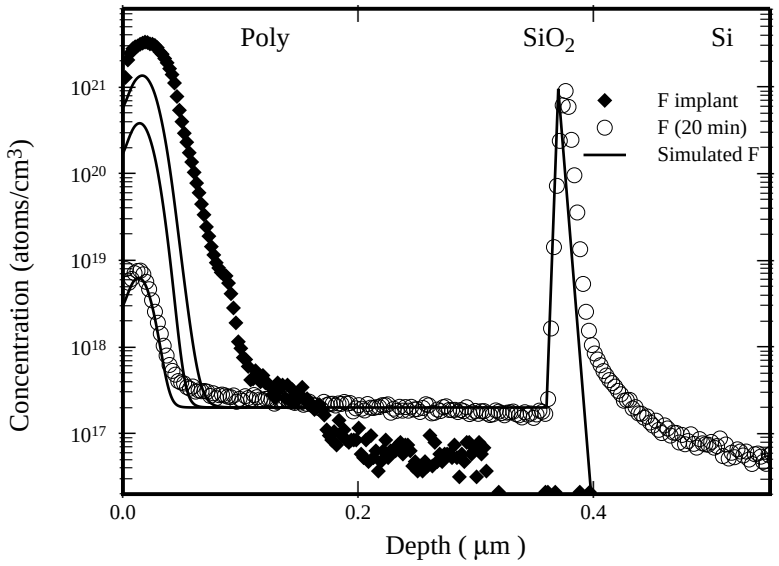

Figure 5.2: Comparison of model for fluorine redistribution with SIMS data of oxide grown in 100% O_2 and BF_2 implanted polysilicon annealed for 20 min at 950°C.

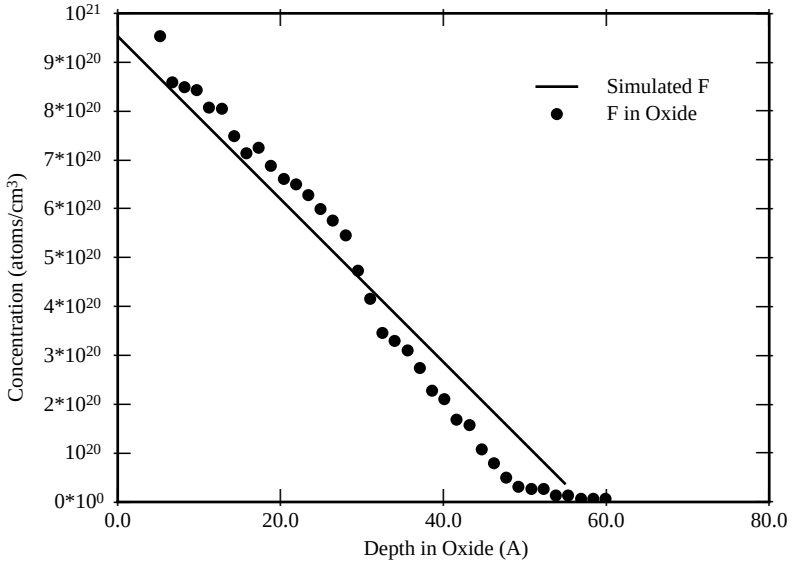

Figure 5.3: Comparison of simulated fluorine with SIMS data in oxide grown in 100% O_2 with BF_2 implanted polysilicon annealed for 20 min.

where k is the reaction rate of fluorine atoms to form clusters and C_{ss} is the solid solubility of fluorine in polysilicon.

When fluorine concentration is larger than the solid solubility limit (2×10^{17} cm^{-3}) clusters form and grow. When fluorine concentration is below the solid solubility clusters dissolve and fluorine diffuses. Fluorine profiles in oxide are determined by diffusion and segregation at both interfaces. Figure 5.2 shows the simulation results in polysilicon compare to SIMS data. Figure 5.3 shows the profile of fluorine in oxide for the same simulation.

The shortcoming of above model is that it predicts a nearly linear dissolution of aggregated fluorine in polysilicon. However, close inspection of Figure 5.1 shows that even after 80min anneal the fluorine aggregates are still present. One may conclude that a ripening model should be implemented to account for this behavior. In addition, the top oxide layer may be a source of fluorine at longer times.

5.4 Conclusions

We investigated the role of fluorine redistribution in the poly/SiO_2/Si system. Although nitrogen incorporation is fairly uniform in the gate dielectric, the profile of fluorine shows a linear behavior. This suggests that fluorine diffuses readily through the gate oxide. Its distribution in the oxide thus depends on the segregation from the poly to the oxide and its concentration in the poly. For short times, the concentration in the poly and oxide remain constant as function of time, but as fluorine is lost to the substrate and over layers its concentration eventually reduces. This could be an explanation for the reported thickness dependence of boron diffusivities in fluorinated oxides. We implemented a one moment clustering model for diffusion of fluorine in polysilicon and compared results with experimental data.

Chapter 6

Conclusions and future work

6.1 Summary

The goal of this thesis was to gain a fundamental understanding of boron diffusion in gate oxides, specifically the effect of impurity incorporation and the role of grown-in stress. We conducted a series of experiments to characterize boron diffusion in gate dielectrics as a function of incorporated nitrogen fluorine and stress. We also developed models at both the atomistic and continuum level to account for boron penetration over a range of process conditions, as well as stress evolution during oxidation of silicon.

First, we presented a model describing the evolution of stress in planar oxides. As shown by the relaxation data of Landsberger and Tiller [4], oxides grown at lower temperature tend to exhibit higher refractive indexes which translates into higher densities. When annealed, these oxide structures dilate with an accompanying reduction in their index of refraction. From these observations, we concluded that excess oxide density is relaxed during annealing. We proposed a viscous compressible model in which a dense oxide is generated at the Si/SiO_2 interface and is then relaxed by solving the mass and momentum balance as described in Chapter 2, with a viscosity dependent on the local excess density. This model predicts a nonuniform distribution of excess density through out the oxide, with larger excess density near the Si/SiO_2 interface. The model was then extended to account for the two step oxidation experiments of Landsberger and Tiller [5], which found that oxides which are originally grown at lower temperatures show a slower growth rate upon reoxidation compared to oxides initially grown at higher temperatures. Our model accounted for this behavior by assuming that the diffusivity as well as solubility of oxidizing species depend on the local excess density. That is, for oxides that have higher excess density (oxides grown at lower temperatures) diffusivity and solubility of the oxidizing species are reduced. At higher temperatures the viscosity of the oxide is reduced (viscosity of oxide is highly activated with 7.4 eV activation energy [60]) resulting in overall lower excess density. With this model, we were able to account for the two step oxidation results [4] and extracted new stress-dependent parameters for the oxidation of silicon. We were also able to predict the growth kinetics of the thin oxide regime. The model was extended to account not only for $\langle 111 \rangle$ but also to include data [8] for $\langle 100 \rangle$ silicon.

The remainder of this thesis addressed the issue of boron penetration through gate oxides. Experiments were designed and carried out to characterize boron diffusion under a range of conditions. First, oxides with different thermal history were grown to explore the effect of excess density on boron diffusion. The most significant outcome of this experiment was to realize that a relaxed oxide, one that had been grown at a lower temperature (800°C) and then annealed at a higher temperature (1100°C), showed significantly larger boron diffusivity ($\sim$4 times) compared to an oxide that had seen no high temperature anneal. To model this behavior, we assumed that boron diffusivity is reduced with density, and an activation volume of 27Å^3 was extracted for boron diffusion in oxide.

We also examined boron diffusion through dielectrics grown in the presence of nitrogen. It has been shown [11, 9, 65] that boron diffusion is reduced in oxynitride dielectrics. Most work to date has focused on reporting an effective diffusivity for boron diffusion in gate dielectrics. In this work we not only extracted an effective diffusivity in various gate dielectrics but also carried out SIMS measurement to study the incorporated impurity in gate oxide. With this approach, we were able to relate boron diffusion through the gate dielectric to the local impurity (nitrogen and fluorine) incorporated in the gate dielectric. We also reported our effective diffusivity parameters for comparison with other work in literature. Comparison of our data with Aoyama *et al.* (the most extensive set of experiments in the literature) shows very similar activation and preexponential factors for boron diffusion in different dielectrics. In addition we investigated boron penetration for oxynitride gate dielectrics with different amounts of nitrogen incorporation. The results show that a significant amount of nitrogen ($> 1\%$) is required to substantially reduce boron penetration.

Boron diffusion is known to increase in presence of fluorine. To further investigate this effect we implanted the gate polysilicon with BF_2 and extracted boron diffusivity in both oxide and oxynitride films. Again SIMS measurement were carried out to extract the profile of incorporated fluorine in gate oxides.

Boron exhibits substitutional diffusion behavior in gate dielectric and its diffusivity is modified by the structure of oxide. Boron diffusivity is increased in the presence of network terminator species like fluorine or hydrogen and is reduced in presence of network former species like nitrogen. To develop a model for this behavior we used lattice Monte Carlo simulations in which boron atoms diffused through a quartz-like structures in the presence of either fluorine or nitrogen, which locally enhanced or retarded the boron hopping rate. The results of these simulations were used as the basis of a continuum model, which was then fitted to experimental data and diffusion parameters were extracted.

Finally, to better understand the kinetics of fluorine incorporation we carried out experiments where BF_2 implanted poly/oxide/Si structures were annealed for various times and SIMS measurements were carried out to better understand the distribution of fluorine in the poly/oxide/Si structure. SIMS measurements revealed that fluorine has a low solubility but fast diffusivity in both silicon and polysilicon. It segregates very strongly to the gate dielectric. The profile of fluorine in the gate is determined by the concentration in polysilicon and the segregation coefficient in oxide. Another feature that was observed is the presence of an immobile peak, most likely fluorine aggregates, near the initial fluorine implant. These aggregates seem to dissolve very fast initially but form a stable phase where they remain insoluble for much longer annealing times.

6.2 Future Work

There are many interesting questions still open concerning both the oxidation process as well as boron penetration in gate dielectrics. Among the issues that need to be resolved is the extension of the viscous compressible model of oxidation to two dimensions. The proper course of action would be to test the model on the experimental work of the type obtained by Kao *et al.* [50] from the cylindrical oxidation. Also, it would be very interesting to extend the stress generation and relaxation model to try to predict the stress evolution in oxynitride or oxides in presence of network terminator species like fluorine and hydrogen. Nitrogen, fluorine and hydrogen are known to modify the structure of the oxide and can have direct bearing on the structurally-dependent oxidation parameters as well as the mechanical parameters, specifically the viscosity of oxide.

Further experiments would be useful to better characterize boron diffusivity as a function of excess density SiO_2. These experiments should address different anneal temperatures and times. Oxide grown at low temperatures should be annealed at various times and temperatures to produce oxides with different excess density distributions. These oxide should then be used to more accurately characterize boron diffusion as a function of excess oxide density.

Experiments to further examine the effect of nitrogen incorporation on boron diffusion would also be worthwhile. In this work we examined effect of nitrogen incorporation for oxynitrides grown in 100% as well as 20% N_2O ambients. Both intermediate as well as higher levels of nitrogen incorporation should be investigated. These oxides can then be used to quantify boron penetration as function of percent nitrogen incorporation.

As fabrication technology moves towards faster and smaller devices, many new processes are developed. Among these new innovations are the use of novel methods to grow thinner and more reliable gate dielectrics. Examples are such processes are oxidation of the N-implanted silicon [77] or very thin stack gate (ONO) and other high κ dielectrics. Experimental must be carried out to better understand the interaction of these films with dopant diffusion and impurity incorporation. Furthermore application of atomistic calculation (LMC and/or LDA) is essential to guide modeling of these phenomena.

Appendix A

Numerical Methods

To describe oxidation, a set of partial differential equations representing the oxidant diffusion and oxide flow must be solved, as discussed in Chapter 2. These PDEs cannot easily be solved analytically and therefore numerical techniques are essential. The most general way of solving these equations is to create a grid and rewrite the equations for each domain. The goal is to solve the oxidation and flow equations using finite element methods. This will change the PDEs to a set of algebraic equations that can be solved by Gaussian elimination. If the equations are not linear they should be linearize before solving.

A.1 Finite Elements Approach

The FEM (finite element method) obtains an approximate solution by using the classical *trial-solution* procedure. If we assume that a differential equation has a solution function $U(x)$ (in 1D) then FEM will result in a function $\tilde{U}(x)$ which only approximately satisfies the governing equations and boundary condition.

The trial-solution procedure can be characterized by three principal operations:

1. Construction of a trial solution for $\tilde{U}$.
2. Application of an optimizing criterion to $\tilde{U}$.
3. Estimation of accuracy of $\tilde{U}$.

A.1.1 Shape functions

The first operation involves the construction of a trial solution $\tilde{U}(x;a)$ which is in the form of finite sum:

$$\tilde{U}(x;a) = \sum_{i=0}^{n} \phi_i(x) a_i \tag{A.1}$$

Here, x represents all the independent variables in the problem. The functions $\phi_i(x)$ are known functions called shape functions. The coefficients a_i are undetermined parameters.

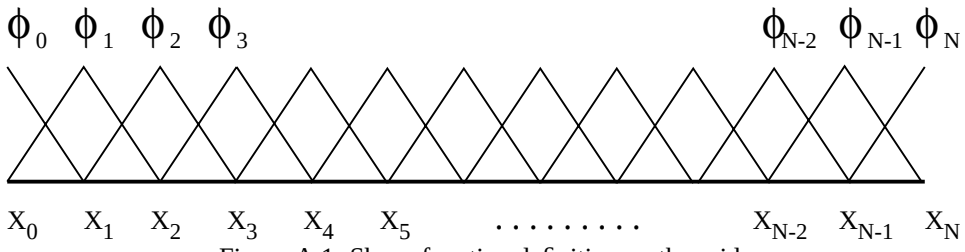

Figure A.1: Shape function definition on the grid.

The construction of a trial solution consists of constructing an expression for each of the shape functions. From a practical standpoint it is important to use functions that are algebraically as simple as possible and are also easy to work with. An example of such a function is shown in Figure A.1.1. The properties of these shape functions can be summarized as:

1. $\phi_i(x_j) = \begin{cases} 1 & \text{if i=j} \\ 0 & \text{otherwise} \end{cases}$
2. $\phi_i(x) * \phi_j(x) = 0 \quad \text{for} \quad |\,\text{i - j}\,| > 1$
3. $\phi_i'(x) * \phi_j'(x) = 0 \quad \text{for} \quad |\,\text{i - j}\,| > 1$
4. $\phi_i(x) * \phi_{i+1}(x) = \begin{cases} \frac{(x_{i+1}-x)(x-x_i)^2}{(x_{i+1}-x_i)^2} & \text{on } [x_i, x_{i+1}] \\ 0 & \text{elsewhere} \end{cases}$
5. $\phi_i'(x) * \phi_{i+1}'(x) = \begin{cases} -1/(x_{i+1}-x_i)^2 & \text{on } [x_i, x_{i+1}] \\ 0 & \text{elsewhere} \end{cases}$

The Next step is to determine a specific numerical value for each of the parameters a_i in Equation A.1. This is done by minimizing the error of the differential equation (application of an optimizing criterion). There are many different types of optimizing criteria to choose from. Collocation, subdomain, least square and Galerkin method are examples of such optimization. Of these, the Galerkin residual method has been used in most FEM works. All problems in the remainder of this work will employ the Galerkin method.

The next section will explain the application of finite element for oxidation. The shape function and approximate solution will be formulated. This formulation is then minimized using the Galerkin method producing a set of linear algebraic equations that can be solve by Gaussian elimination.

A.2 Oxidation Equation

For the time being lets assume that mechanical equations can be ignored. The only equation describing oxidation then is:

$$\frac{\partial C}{\partial t} + \nabla \cdot (\mathbf{j} + C\mathbf{v}) = 0 \tag{A.2}$$

where the flux **j** is:

$$\mathbf{j} = -D\nabla C. \tag{A.3}$$

and C is the concentration of O_2 and **v** is the velocity. Assuming steady state and ignoring the $\nabla(C\mathbf{v})$ term we have:

$$\nabla \cdot (DC) = 0 \tag{A.4}$$

The search for the solution proceeds by writing the approximate solution function $\tilde{C}$ as a sum of unknown coefficients times known functions ϕ_i:

$$\tilde{C} = \sum_{i=0}^{n} \phi_i(x) a_i. \tag{A.5}$$

Applying the above sum to Equation A.4 and using Galerkin minimization routine:

$$\int_\Omega \frac{\partial}{\partial x} D \frac{\partial \tilde{C}}{\partial x} \phi_j(x) dx = 0. \tag{A.6}$$

Integrating by parts the above equations become:

$$\int_\Omega \frac{\partial \tilde{C}}{\partial x} D \frac{\partial \phi_j(x)}{\partial x} dx = -(-D\frac{\partial \tilde{C}}{\partial x})\,\phi_j(x)\Big|_{\Gamma_R} \tag{A.7}$$

Plugging Equation A.5 in above:

$$\int_\Omega \sum_{i=0}^{n} a_i \frac{\partial \phi_i(x)}{\partial x} D \frac{\partial \phi_j(x)}{\partial x} dx = -(-D\frac{\partial \tilde{C}}{\partial x})\,\phi_j(x)\Big|_{\Gamma_R} \tag{A.8}$$

where a_i are the unknown coefficients of the solution. In the finite element method the basis is finite of order N, so there are N unknowns. The above formulation is applied for $j = 0 \ldots N$ leading to N equations and N unknowns. The partial differential equation is thus transformed into a set of algebraic equations for unknowns a_i. In this case the set of equations and their unknowns can be solved by Gaussian elimination [78].

A.3 Flow Equations

Let's add the mechanical equations and try to solve the complete set.

$$\frac{\partial C}{\partial t} + \frac{\partial}{\partial x}(D\frac{\partial C}{\partial x} + C\mathbf{v}) = 0 \tag{A.9}$$

$$\frac{\partial \rho}{\partial t} + \frac{\partial(\rho \mathbf{v})}{\partial x} = 0, \tag{A.10}$$

$$\rho\frac{\partial v}{\partial t} + \rho v\frac{\partial v}{\partial x} - \frac{\partial \sigma}{\partial x} = 0, \tag{A.11}$$

$$\sigma = -P + (\lambda + 2\mu)\frac{\partial V}{\partial x}, \tag{A.12}$$

Equations A.10 and A.11 can be discretized in the same manner as previous section. These two equations are coupled time dependent partial differential equations. Once the equations are discretized a simple "plug-in"

iteration method is used to calculate the velocity and density vectors in the above equations. An initial guess (usually the value from the previous time step) is used for the density distribution. From this initial guess the velocity vector is calculated for the existing grid where it is used to compute the density distribution and so on. For the time discretization, an implicit scheme has been used. Typically 5-6 iterations are sufficient to reduce the norms of the errors. A simple time stepping routine is implemented where the velocity and density vectors are calculated for a full time step and compared to those for two half time steps.

A.4 Moving Boundary Problem

The difficulty associated with this problem is the problem of the moving interface. As described in chapter 2, the solution to Eq. A.2 provides the boundary conditions for the velocity. However, instead of generating a large volume of unstressed oxide, we assume that a region of high stress is created with the same volume as the silicon consumed and density

$$\rho = m_{ox} C_{si}, \tag{A.13}$$

This high density region is relaxed by solving the coupled partial differential equations of mass and momentum balance, which also contribute to the growth of the oxide. However, due to the nonlinearity dependence of viscosity

$$\mu = \mu_0 \, \frac{(\rho - \rho_0)/(\sigma_c \, \rho_0)}{\sinh((\rho - \rho_0)/(\sigma_c \, \rho_0)}. \tag{A.14}$$

and high value of ρ at the interface, previously described numerical methods behave poorly in solving the equations for this system.

To address this issue we implemented a routine where upon calculation of velocity at the interface, the interface density is relaxed by solving the analytic equation:

$$\mu_0 \left(\frac{-\lambda \rho^T/\sigma_c}{\sinh(-\lambda \rho^T/\sigma_c)} \right) \frac{\partial \rho^T}{\partial t} = -\lambda \rho^T \tag{A.15}$$

with

$$\rho^T = \frac{\rho^i - \rho_0}{\rho_0} \tag{A.16}$$

where ρ^i is the density at the interface grid point and ρ_0 is the equilibrium oxide density. The nonlinear equation reduces to:

$$\int \frac{\partial \rho^T}{\sinh(-\lambda \rho^T/\sigma_c)} = \int \frac{\sigma_c \, \partial t}{\mu_0} \tag{A.17}$$

The integral can be evaluated using a standard substitution, q=tanh$(r/2)$.

$$\frac{\sigma_c}{\lambda} \ln\left(\tanh(\lambda \, \rho^T/2\sigma_c)\right) = -\sigma_c t/\mu_0 \tag{A.18}$$

Finally the relaxed density at the interface can be calculated directly:

$$\rho^i = \frac{2\rho_0\sigma_c}{\lambda}\tanh^{-1}(\exp(-t\lambda/\mu_0)) + \rho_0 \tag{A.19}$$

The time associated with relaxation of the interface point is calculated by determining the time required to grow a monolayer of oxide given the interface velocity. This time is then substituted in the above equation and the relaxed interface density is calculated. It is apparent that this relaxation must give rise to the dilation of oxide, therefore the velocity associated with this relaxation is used to move the grid in the oxide contributing to oxidation.

Appendix B

Experimental Procedures

A variety of silicon dioxide and oxynitrides with different amount of nitrogen incorporation were evaluated in this work. These dielectrics were grown in several IC fabrication facilities, using a range of processing conditions and techniques. Gate dielectric were grown on bare silicon wafers to study their chemical and material properties. The same gate dielectrics were incorporated into capacitor structure to evaluate the amount boron penetration associated with each dielectric. Figure B.1 illustrates the the structures used in this work. This chapter outlines the process flows for the fabrication of the MOS capacitors and describes the specific conditions used for gate dielectric fabrication.

B.1 Process Flow

The starting wafer for all experiments were *n*-type, 100 CZ wafer, 20–100 Ω-cm, 19–21 mils thick. The gate dielectrics were fabricated using pure O_2, pure N_2O and 20/80% N_2O/O_2 (the later two processes were performed at the Microelectronic Laboratory of the University of Texas at Austin). For the stress experiments the dielectric plus the deposited polysilicon were annealed at 1100°C for 20 minute to examine the effect of stress relaxation on boron diffusion in oxide.

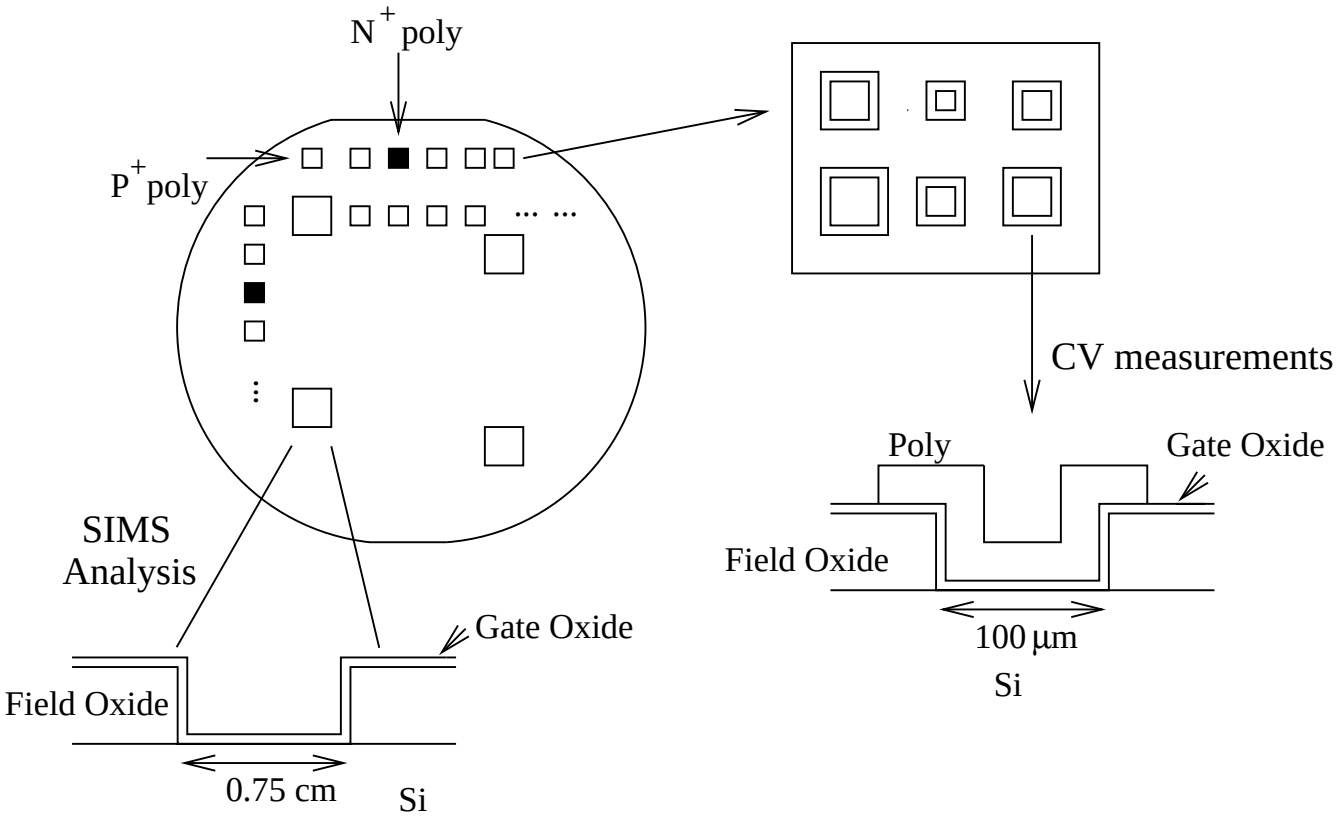

Figure B.1: Illustration of structures fabricated for investigation of boron penetration in gate dielectrics.

Step #	Step Name	Description
1	Field Oxide 660 nm	RCA 1000°C wet O_2 recipe 122
2	Active Area Pattern	
3	Oxide Wet Etch	BOE 6 min
4	Resist Strip	
5	Gate Oxidation	As noted in text
6	Poly Deposition (LPCVD)	625°C 3000Å recipe 461, 40 min
7	Resist Coat	
8	Backside Poly Plasma Etch	Recipe 10, CCl_4
9	Backside As Implant	5e15, 40 keV
10	Resist Strip	
11	Front Side Pattern PMOS Capacitors	
12	Boron or BF_2 Implant	5e15, 25 keV

Step #	Step Name	Description
13	Resist Strip	
14	Front Side Pattern NMOS Capacitors	
15	Phos Implant	5e15, 40keV
16	Resist Strip	
17	Deposit LTO 5000Å	
18	Anneal in N_2	Various Times and Temps
19	BOE LTO oxide Removal	4 min
20	Polysilicon Pattern	Recipe 10, CCl_4
21	Polysilicon Plasma Etch	
22	Resist Ash	

B.2 Capacitance Voltage Measurements

Capacitor devices were evaluated using capacitance-voltage (CV) measurements. High-frequency CV curves were measured at 100 kHz, using an HP4275 LCR meter with the bias driven externally by an HP4145 Semiconductor Parameter Analyzer. The capacitance was measured every 50 mV as the bias was swept from inversion to accumulation. The parasitic capacitance of the probe-station set up was subtracted from the measured data.

The dielectric thickness was extracted from the maximum high-frequency capacitance on the CV curve, assuming a dielectric constant of $\varepsilon = 3.9\varepsilon_0$. This value agreed with the ellipsometry measurements following the gate oxidation on a dummy wafer (within $\pm$10%). An array of 3×2 capacitors with dimensions ranging from 20×20 to 120×120 μm were fabricated. The measurements were carried out on the 100×100 μm capacitors.

When boron diffuses into the n-type substrate and counterdopes the channel, V_{FB} deviates from its ideal value according to:

$$V_{FB} = \phi_{ms} + \frac{q(N_B - N_F)}{C_{ox}} \tag{B.1}$$

where ϕ_{ms} is the ideal metal-semiconductor work function, q is the electron charge, and C_{ox} is the areal oxide capacitance, i.e. the dielectric permittivity ε_{ox} divided by the oxide thickness t_{ox}. The penetrated boron, N_B, is defined as the effective density of boron which has diffused into the channel and N_F is the density of positive fixed charge in the oxide. Positive fixed charge causes a negative shift in flatband voltage, while boron penetration will shift V_{FB} to a more positive value.

Figure B.2 compares the flatband voltages of MOS capacitors with $\sim$ 50Å 950°C N_2O and O_2-grown gate dielectrics, for different gate dopant species and post-implant annealing times. The good agreement between the ideal and measured CV curves for phosphorus doped polysilicon samples indicates that the fixed charge density is low in these samples and that any positive shift in V_{FB} observed with p-type polysilicon can be attributed to boron penetration.

Across wafer oxide thickness variation measured by ellipsometry and extracted from CV curves were within $\pm$ 10 %. However variation of the shift of flat band voltages were larger on some samples specifically the CV curves measured for the study of stress on boron penetration. To provide a good statistics CV measurements were carried out for at least 20 different MOS capacitors on each wafer.

The boron diffusivities associated with the voltage shifts in the CV curves were determined through a series of linked SUPREM IV and PISCES simulations. Effective diffusivity is defined as the boron diffusivity in oxide in the SUPREM simulations for which the PISCES simulation best matched the measured CV curves. The results of these simulations show that the CV measurement technique is very sensitive to extracted boron diffusivity in oxide. Figure B.3 shows two CV curves for oxides grown in 100% N_2O with BF_2 implanted polysilicon. Also shown are the extracted diffusivities which demonstrates the sensitivity to the shift of the CV curves.

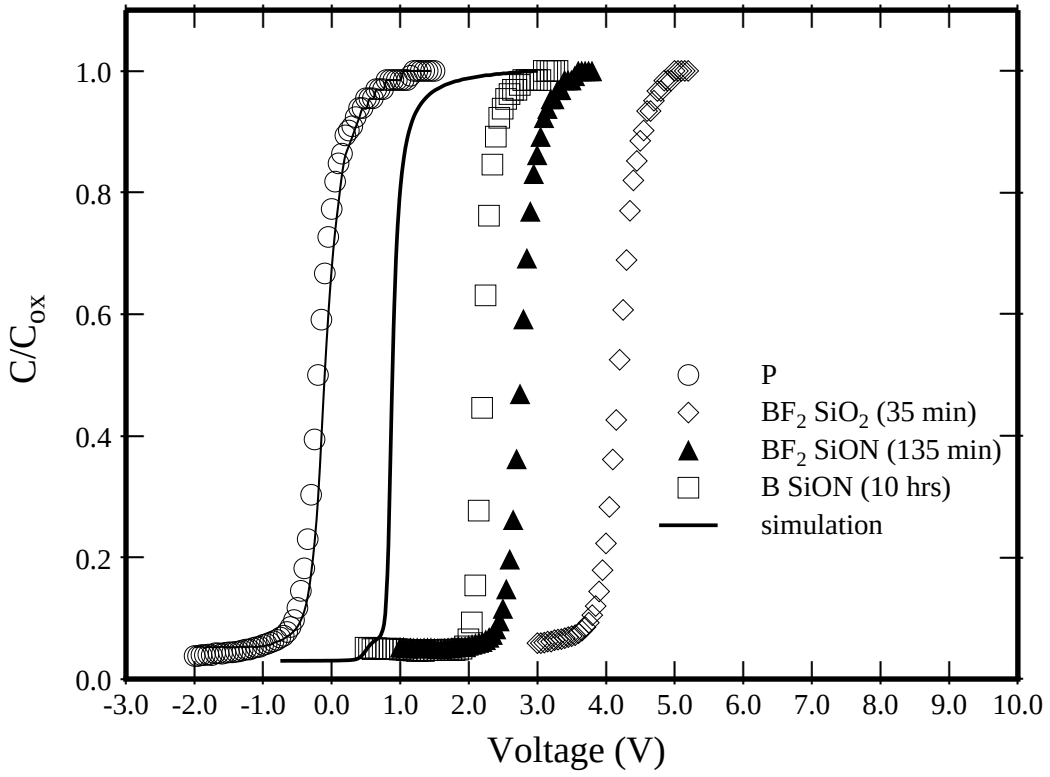

Figure B.2: Capacitor-Voltage measurement results for samples with different gate dielectrics annealed at 950°C. Also included are the monitor phosphorus and boron doped capacitors. Lines are the simulated process/device simulation for all conditions and p^+-doped capacitor with no boron penetration.

B.3 Secondary Ion Mass Spectroscopy

Secondary ion mass spectroscopy (SIMS) is an inherently destructive atomic identification technique in which surface atoms are sputtered off the material being analyzed and their mass-to-charge ratio determined. It is remembered as the "ions-in, ions-out" approach. A primary beam of ionized atoms is directed at a surface, and through billiard-ball-like collisions, surface atoms are knocked loose and ionized (see figure B.4. Charged species which are removed from the sample surface are directed into a mass spectrometer for identification. Since the SIMS technique simultaneously sputters the surface, the time scale is directly convertible to a depth scale. Special precautions were taken to ensure adequate depth resolution of ultra-thin dielectric films. One important consideration was the choice of sputtering ion species. In this work, we explored the use of both cesium (Cs^+) and oxygen ($O_2{}^+$) ions for sputtering.

The SIMS analysis in this work were done at Evans East Inc. $O_2{}^+$ primary ion bombardment was used with positive secondary ion detection to measure the boron profiles in oxide. A physical Electronics Model

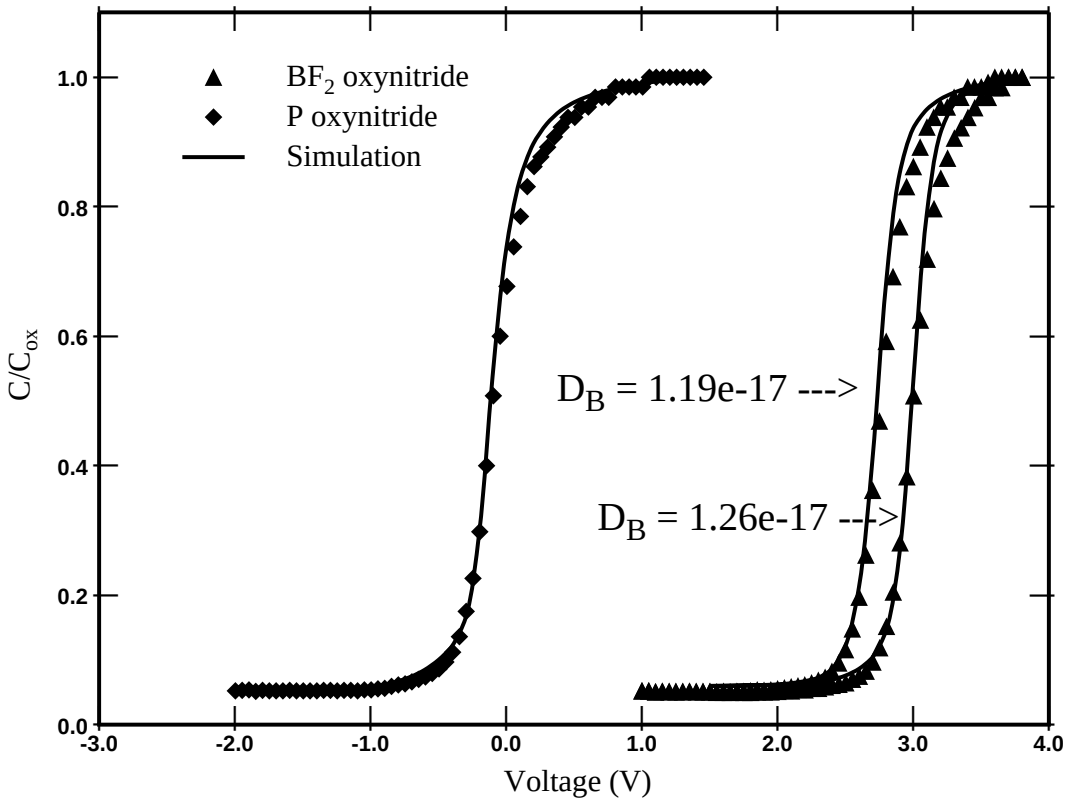

Figure B.3: Comparison of simulation with CV measurements for BF_2/oxynitride sample (D_B=1.2e-17 at 950°C)

6300 Secondary Ion Mass Spectrometer was used for these analysis. For nitrogen and fluorine profiles, Cs^+ primary ion bombardment was used with positive secondary ion detection. These measurements were carried out on a Physical Electronics Model 6600 SIMS.

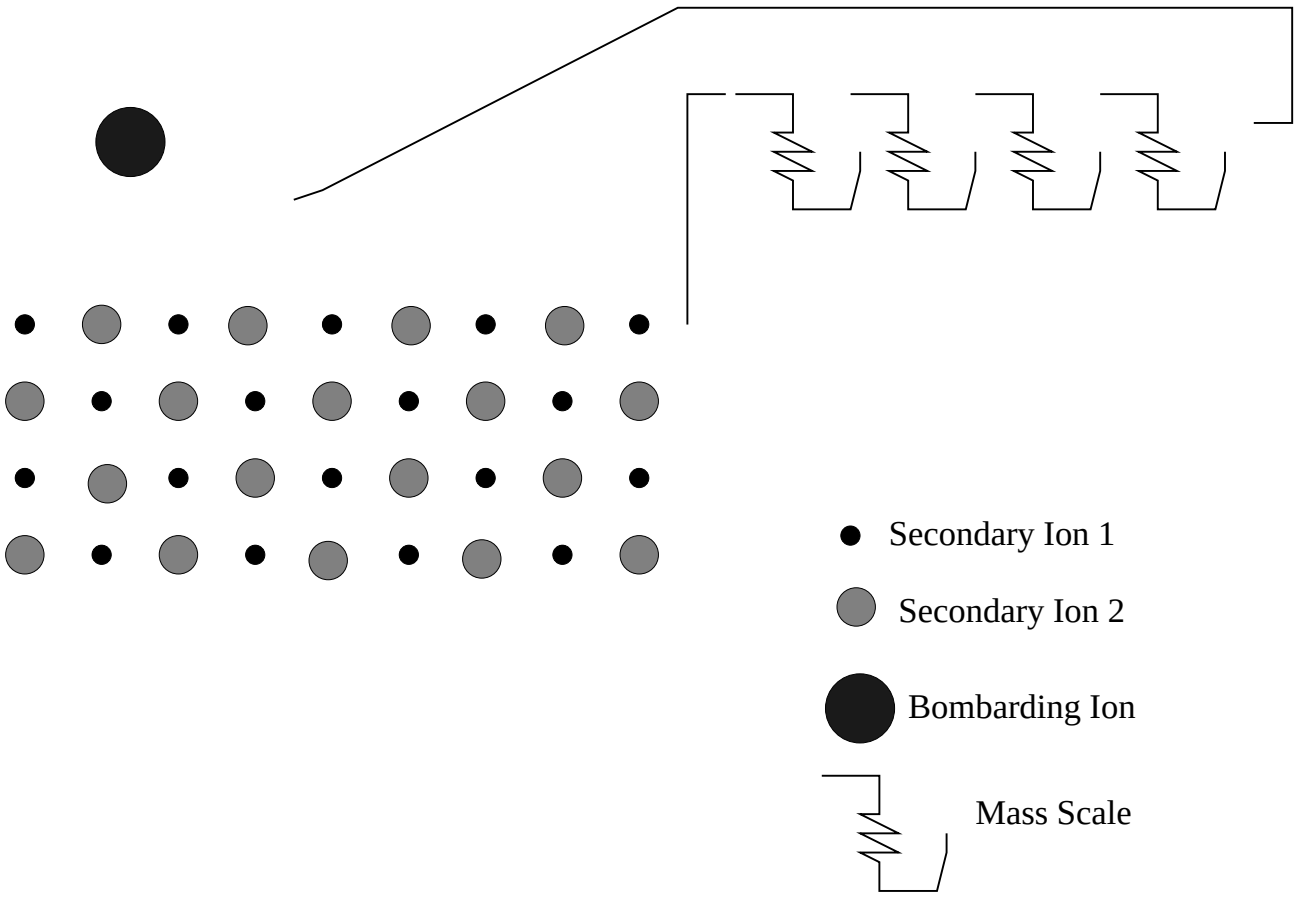

Figure B.4: Secondary Ion process, bombarding ion knocks the atoms off the surface and Mass Spectrometer separates the atoms based on their mass-charge ratio

Bibliography

[1] C. S. Rafferty, L. M. Landsberger, R. W. Dutton, and W. A. Tiller. Nonlinear viscoelastic dilation of SiO_2 films. *Appl. Phys. Lett.*, 54(2):151, 1989.

[2] E. A. Taft. The optical constants of silicon and dry oxygen oxides of silicon at 5461a. *J. Electrochem. Soc.*, 125:968, 1978.

[3] I. H. Malitson. Interspecimen comparison of the refractive index of fused silica. *J. Opt. Soc. America*, 55:1205, 1965.

[4] E. A. Irene. Silicon oxidation studies: Some aspects of the initial oxidation regime. *J. Electrochem. Soc.*, 125:1708, 1978.

[5] L. M. Landsberger and W. A. Tiller. Refractive index, relaxation times and the viscoelastic model in dry-grown SiO_2 films on Si. *Appl. Phys. Lett.*, 51(18):1416, 1987.

[6] L. M. Landsberger and W. A. Tiller. Two-step oxidation experiments to determine structural and thermal history effects in thermally-grown SiO_2 films on Si. *J. Electrochem. Soc.*, 137(9):2825, 1990.

[7] C. J. Han and C. R. Helms. Parallel oxidation mechanism for si oxidation in dry O_2. *J. Electrochem. Soc.*, 134:1299, 1987.

[8] H. Z. Massoud, J. D. Plummer, and E. A. Irene. Thermal oxidation of silicon in dry oxygen: Growth rate enhancement in the thin regime i. experimental results. *J. Electrochem. Soc.*, 132(7):1745, 1985.

[9] K. Taniguchi, M. Tanaka, C. Hamaguchi, and K. Imai. Density relaxation of silicon dioxide on (100) silicon during thermal annealing. *J. Appl. Phys.*, 67(5):2195, 1990.

[10] K. S. Krisch, M. L. Green, F. H. Baumann, D. Brasen, L. C. Feldman, and L. Manchanda. Thickness dependence of boron penetration through O_2 and N_2O-grown gate oxides and its impact on threshold voltage variation. *IEEE Transactions on Elect. Devices*, 43(6):982, 1996.

[11] C. Subramanian, Jim Hayden, W. Taylor, M. Orlowski, and T. McNelly. Reverse short channel effect and channel length dependence of boron penetration in pmosfets. In *IEDM Tech. Digest*, pages 17.3.1–17.3.4, 1995.

[12] T. Aoyama, K. Suzuki, H. Tashiro, Y. Toda, T. Yamazaki, K. Takasaki, and T. Ito. Effect of fluorine on boron diffusion in thin silicon dioxides and oxynitride. *J. Appl. Phys.*, 77(1):417, 1995.

[13] K. A. Ellis and R. A. Buhrman. Monte carlo simulation of boron diffusion is silicon oxides and oxynitrides. In *Electrochem. Society Symposium*, pages 285–296, 1997.

[14] T. Morimoto, H. Momose, Y. Ozawa, K. Yamabe, and H Iwai. Effects of boron penetration and resultant limitation in ultra thin pure-oxide and nitrided-oxide gate-films. In *IEDM Tech. Digest*, page 429, 1990.

[15] C. Y. Wong and F. S. Lai. Ambient and dopant effects on boron diffusion in oxides. *Appl. Phys. Lett.*, 48(24):1658, 1986.

[16] Y. S. Diamand and W. G. Oldham. The effect of hydrogen on boron diffusion in SiO_2. *J. Electronic Materials*, 15:229, 1986.

[17] H. A. Schaeffer. Oxygen and silicon diffusion-controlled processes in vitreous silica. *J. Non. Crys. Solids*, 38:545, 1980.

[18] B. E. Deal and A. S. Grove. General relationship for the thermal oxidation of silicon. *J. Appl. Phys.*, 36:3770, 1965.

[19] E. P. EerNisse. Stress in thermal SiO_2 during growth. *Appl. Phys. Lett.*, 35(1):8, 1979.

[20] L. M. Landsberger. *Structural Relaxation Effects in Dry Thermally-Grown Silicon Dioxide Films on Silicon*. PhD thesis, Stanford University, June 1988.

[21] J R. Pfiester, F. K. Baker, T. C. Mele, H. Tseng, P. J. Tobin, and J. D. Hayden. The effect of boron penetration on p^+ polysilicon gated pmos devices. *IEEE Trans. Electron Devices*, 37(8):1842, 1990.

[22] A. Uchiyama, H. Fukuda, T. Hayashi, and S. Ohno. High performance dual-gate sub-halfmicron CMOSFETs with 6 nm-thick nitrided SiO_2 films in an N_2O ambient. In *IEEE Int. Electron Device Meeting Tech Digest*, page 425, 1990.

[23] R. E. Loehman. Oxynitride glasses. *MRS Bulletin*, pages 26–30, 1987.

[24] C. Lin, A. I. Chou, P. Choudhury, and J. C. Lee. Effect of BF_2 implantation on ultrathin gate oxide reliability. *J. Amer. Inst. of Phys.*, 38:545, 1980.

[25] H. Hwang, W. Ting, D. Kwong, and J. Lee. A physical model for boron penetration through an oxynitride gate dielectric prepared by rapid thermal processing in N_2O. *Appl. Phys. Lett.*, 59(13):1581, 1991.

[26] R. P. Vasquez and A. Madhukar. Distribution of nitrogen and defects in SiO_xN_y/Si structures formed by the thermal nitridation of SiO_2/Si. *Appl. Phys. Lett.*, 46(4):1658, 1985.

[27] G. Q. Lo, W. Ting, and D. L Kwong. Improved performance and reliability of mosfets with ultrathin gate oxides prepared by conventional furnace oxidation of si in pure N_2O ambient. In *IEEE Int. Electron Device Meeting Tech Digest*, page 425, 1990.

[28] D. Mathiot, A. Straboni, E. Andre, and P. Debenest. Boron diffusion through thin gate oxides: Influence of nitridation and effect on the Si/SiO_2 interface electrical characteristics. *J. Appl. Phys.*, 73(12):8215, 1993.

[29] M. Bhat, J. Ahn, and D. L. Kwong. Comparison of the chemical structure and composition between N_2O oxides and reoxidized NH_3-nitrided oxides. *Appl. Phys. Lett.*, 64(9):1168, 1994.

[30] R. I. Hegde, B. Maiti, and P. Tobin. Growth and film characteristics of N_2O and NO oxynitride gate and tunnel dielectrics. *J. Electrochem. Soc.*, 144:1081, 1997.

[31] T. S. Chao, W. H. Chen, S. C. Sun, and H. Y. Chang. Characterizations of oxide grown by N_2O. *J. Electrochem. Soc.*, 140:2905, 1993.

[32] E. C. Carr and R. A. Buhrman. Effects of nitrogen incorporation in thin silicon oxides grown in N_2O. In *TECHON'93, Atlanta*, page 234, Sept 1993.

[33] U. S. Kim, C. H. Wolowodiuk, and R. J. Jaccodine. The effect of fluorine additions to the oxidation of silicon. *J. Electrochem. Soc.*, 137:2291, 1990.

[34] D. Kouvatsos, J. Huang, and R. J. Jaccodine. Fluorine-enhanced oxidation of silicon. effects of fluorine on oxide stress and growth kinetics. *J. Electrochem. Soc.*, 138:1752, 1991.

[35] M. Morita, T. Kubo, T. Ishihara, and M. Hirose. Fluorine-enhanced thermal oxidation of silicon in the presence of NF_3. *Appl. Phys. Lett.*, page 1312, 1981.

[36] T. P. Ma. Metal-oxide-semiconductor gate oxide reliability and the role of fluorine. *J. Vac. Sci. Technol. B*, 10:705, 1992.

[37] E. Cartier, J. H. Stathis, and D. A. Buchanan. Passivation and depassivation of silicon dangling bonds at the Si/SiO_2 interface by atomic hydrogen. *Appl. Phys. Lett.*, 63:1510, 1993.

[38] R. B. Fair. Physical models of boron diffusion in ultrathin gate oxides. *J. Electrochem. Soc.*, 144:708, 1997.

[39] C. S. Rafferty. *Stress Effects in Silicon Oxidation Simulation and Experiments*. PhD thesis, Stanford University, Dec. 1989.

[40] J. M. Sung, C. Y. Lu, M. L. Chen, and S. J. Hillenius. Fluorine effect on boron diffusion of p+ gate devices. In *IEDM Tech. Digest*, page 429, 1990.

[41] F. K. Baker, J. R. Pfiester, T. C. Mele, H. Tseng, P. J. Tobin, J. D. Hayden, C. D. Gunderson, and L. C. Parrillo. In *IEDM Tech. Digest*, page 443, 1990.

[42] Y. Sato, K. Ehara, and K. Saito. Enhanced boron diffusion through thin silicon dioxide in a wet oxygen atmosphere. *J. Electrochem. Soc.*, 136(6):1777, 1989.

[43] D. M. Brown and P. R. Kennicott. Glass source b diffusion in Si and SiO_2. *J. Electrochem. Soc.*, 118(2):293, 1971.

[44] M. L. Barry and P. Olofsen. Doped oxides as diffusion sources. *J. Electrochem. Soc.*, 116(6):854, 1969.

[45] T. Aoyama, K. Suzuki, H. Tashiro, Y. Toda, Y. Arimoto, and T. Ito. Boron diffusion through pure silicon oxide and oxynitride used for metal-oxide-semiconductor devices. *J. Electrochem. Soc.*, 140(12):3624, 1993.

[46] E. Kobeda and E. A. Irene. In situ stress measurements during thermal oxidation of silicon. *J. Vac. Sci. Technol.*, 7(2):163, 1989.

[47] A. Szekeres and P. Danesh. Mechanical stress in SiO_2/Si structures formed by thermal oxidation of amorphous thermal oxidation of amorphous and crystalline silicon. *Semicond. Sci. Technol.*, 11(8):1225, 1996.

[48] E. A. Irene, E. Tierney, and J. Angilello. A viscous flow model to explain the appearance of high density SiO_2 at low oxidation temperatures. *J. Electrochem. Soc.*, 129(11):2594, 1982.

[49] Y. Sakina, T.Ohno, and S. Matsumoto. Two-dimensional analysis of thermal oxidation of silicon. *Japan. J. Appl. Phys.*, 22:L514, 1983.

[50] D. Kao, J. P. McVittie, W. D. Nix, and K. C. Saraswat. Two-dimensional silicon oxidation experiments and theory. In *IEDM Tech. Digest*, page 388, 1985.

[51] A. Fargeix and G. Ghibaudo. Dry oxidation of silicon: A new model of growth including relaxation of stress by viscous flow. *J. Appl. Phys.*, 54(12):7154, 1983.

[52] Vincent Senez, Dominique Collard, and Bruno Baccus. Analysis and application of a viscoelastic model for silicon oxidation. *J. Appl. Phys.*, 76(6):3285, 1994.

[53] S. Cea and M. Law. Multidimensional nonlinear viscoelastic oxidation modeling. In *Simulation of Semiconductor Devices and Processes, Austria*, volume 6, page 139, Sept 1995.

[54] N. E. McGruer, R. Singh, J. H. Weiss, and K. Rajikanan. In situ anneal-induced growth enhancement during rapid isothermal oxidation of silicon. *J. Appl. Phys.*, 62(8):3405, 1987.

[55] N. Saito, H. Miura, S. Sakata, M. Ikegawa, T. Shimizu, and H. Masuda. A two-dimensional thermal oxidation simulator using vsco-elastic stress analysis. In *IEDM Tech. Digest*, page 696, 1989.

[56] K. Schott, A. Seidl, and J. Lorenz. “two-dimentional simulation of the local oxidation of silicon including the stress effects”. In *Semiconductor Silicon 1990*, pages 417–24, 1990.

[57] W. Merz and N. Strecker. *Math. Method. Appl. Sci.*, 38:545, 1980.

[58] S. Spinner. Elastic moduli of glasses at elevated temperatures by a dynamic method. *J. Am. Ceramic Soc.*, 39:113, 1956.

[59] M. Navi and N. Strecker. Stress during silicon oxidation. In *Meeting of the Electrochemical Society. Miami, Florida*, pages 4.3.1–4.3.4, 1994.

[60] G. Hetherington, K. Jack, and J. Kennedy. The viscosity of vitreous silica. *Phy. and Chem. of Glasses*, 5(5):130, 1964.

[61] F. J. Norton. *Nature*, 171:701, 1961.

[62] H.P. Tuinhout, A. H. Montree, J. Schmitz, and P. A. Stolk. Effects of gate depletion and boron penetration on matching of deep submicron cmos transistors. In *IEDM Tech. Digest*, pages 230–231, 1997.

[63] C. S. Rafferty and R. W. Dutton. Plastic analysis of cylinder oxidation. *Appl. Phys. Lett.*, 54(18):1815, 1989.

[64] M. Navi and S. T. Dunham. Interactions of fluorine redistribution and nitrogen incorporation with boron diffusion in silicon dioxide. In *Inter. Conf. on Sim. of Semi. Proc. and Dev.*, page 335, 1997. M. Law, J. Faricelli and P. Griffin, Cambridge, Mass., USA.

[65] S. Nedelec, D. Mathiot, E. Andre, A. Straboni, and M. Gauneau. Boron diffusion in SiO_2 based dielectric thin layers. In *Silicon Nitride and Silicon Dioxide Thin Insulating Films*, 1985. The Electrochemical Society.

[66] Silvaco International. In *ATHENA and ATLAS User’s Manual*, 1997.

[67] Zhixu Zhou. Boron penetration in dual gate process technology. *Semiconductor Intern.*, 21:89, 1998.

[68] C. Y. Lin, C. Y. Chang, and C. C. Hsu. Suppression of boron penetration in BF_2–implanted p–type gate mosfet by trapping of fluorines in amorphous gate. *IEEE Trans. Electron Devices*, 42:1503, 1995.

[69] S. L. Wu, C. L. Lee, and T. F. Lei. Suppression of the boron penetration induced dielectric degradation by using a stacked–amorphous–silicon film as the gate structure for pmosfet. *IEEE Trans. Electron Devices*, 42:303, 1996.

[70] L. K. Han, D. Wristers, J. Yan, and D. L. Kwong. *IEEE Electron Devics Lett.*, 16:319, 1995.

[71] M. Navi and S. Dunham. Investigation of boron penetration through thin gate dielectrics including role of nitrogen and fluorine. *submitted to J. of Electrochem. Soc.*, 1998.

[72] U. Schnakenberg, W. Benecke, B. Locheland S. Ullerich, and P. Lange. NH_4OH-based etchants for silicon micromachining: influence of additives and stability of passivation layers. *Eurosensors IV '90*, A25:1–7, 1990.

[73] Kathleen S. Krisch. *Mechanisms of Improved Reliability in Reoxidized Nitrided Oxide MOS Gate Dielectric*. PhD thesis, Stanford University, Dec. 1989.

[74] W. B. Fowler and A. H. Edwards. *J. Non. Crys. Solids*, 1997.

[75] Marius Bunea and Scott Dunham. Lattice monte carlo simulation of vacancy-mediated diffusion and aggregation using ab-initio parameters. In *Material Res. Soc.*, 1997.

[76] Alp H. Gencer. In *DOPDEES, Dial-an-Operator Partial Differential Equation Evaluator and Solver*, 1997. Boston University.

[77] C. Lin, A. I. Chou, P. Choudhury, and J. C. Lee. Reliability of gate oxide grown on nitrogen-implanted Si substrate. *App. Phys. Lett.*, 69:3701, 1996.

[78] W. H. Press, S. A. Teukolsky, W. T. Vetterling, and B. P. Flannery. *Numerical Recipes in C The Art of Scientific Computing*. Cambridge University Press, 1992.